





Coordinating behavior of hydrazone ligand bearing chromone moiety towards Cu(II) ions: Synthesis, spectral, density functional theory (DFT) calculations, antitumor, and docking studies

Ebtesam M. Abdelrhman  | B.A. El-Shetary  | Magdy Shebl  |
Omima M.I. Adly 

Department of Chemistry, Faculty of Education, Ain Shams University, Cairo, Egypt

Correspondence

Magdy Shebl, Department of Chemistry, Faculty of Education, Ain Shams University, Roxy, Cairo, Egypt.
Email: magdyshebl@edu.asu.edu.eg

A new hydrazone ligand (FCSH; HL) was successfully synthesized by the reaction of salicylaldehyde hydrazone with 3-formylchromone. Seven copper(II) hydrazone complexes have been synthesized by using several copper(II) salts (acetate, nitrate, sulfate, perchlorate, chloride, and bromide). Elemental analysis, electronic, infrared, mass, nuclear magnetic resonance, electron spin resonance spectra, thermal analysis, molar conductivity, and magnetic susceptibility measurements were used to characterize structures of the hydrazone ligand and its complexes. The ligand behaves as monobasic tridentate for all complexes except complex **2** (monobasic tetradentate) and complex **4** (neutral tridentate). All metal complexes exhibited octahedral geometries. With the aid of Coats–Redfern equations, the kinetic parameters (E_a , A , ΔH , ΔS , and ΔG) of the thermal decomposition stages were calculated and discussed. At the B3LYP/6-311G(d,p) level engaged in the *Gaussian 09* program, density functional theory (DFT) calculations were carried out to inspect the optimized structures of the chelating agent and its complexes. The hydrazone ligand and its copper(II) complexes showed antitumor activity towards HepG2 cell line. The docking study of the hydrazone ligand and its copper(II) complexes was investigated with the active site of the CDK2 kinase.

KEYWORDS

3-formylchromone, antitumor activity, copper(II) complexes, hydrazone, molecular docking

1 | INTRODUCTION

Because of their easy synthesis, excellent complexation with different metal ions and various applications, hydrazones have become a subject of great interest in coordination chemistry. With metal ions, hydrazones form mononuclear and polynuclear (binuclear, trinuclear, and tetranuclear) complexes depending on some factors including (a) nature of the hydrazone ligand

(HL), (b) nature and oxidation state of the metal, (c) the metal to ligand ratio, (d) pH of the medium, and (e) presence of additional donor atoms (usually nitrogen or oxygen) in an appropriate position for chelation.^[1] Hydrazones and their metal complexes possess important applications such as antioxidant,^[2] antimicrobial,^[3] antitumor,^[4] antiviral,^[5] antitubercular,^[6] and antihypertensive^[7] properties as well as other potential applications.^[8]

There is a continuous interest in synthesis of chromones and chromone-based ligands and their complexes because of variable applications of these compounds, namely, antimicrobial,^[9] antitumor,^[10] antiplasmodial and anti-inflammatory,^[11] antioxidant,^[12] and anti-Alzheimer^[13] properties as well as other biological and pharmaceutical applications.^[14]

Synthesis and characterization of copper(II) complexes have been of great interest due to the importance of copper(II) ion in different biological processes. Amongst the first row transition metal complexes, copper complexes have been extensively synthesized because of their important biological and pharmaceutical applications.^[15]

Based on the foregoing facts, the present study aims to investigate the new HL; (3-[(E)-(2E)-(2-hydroxybenzylidene)hydrazinylidene]methyl}-4H-chromen-4-one) (FCSH) derived from the condensation of 3-formylchromone and salicylaldehyde hydrazone. The ligational behavior of FCSH towards copper(II) ion was investigated with focus on the effect of anion on complexation process. Thus, the HL was allowed to react with various copper(II) salts, acetate, nitrate, sulfate, perchlorate, chloride, and bromide, to investigate the effect of these anions on complex formation and properties of the obtained complexes. Characterization of FCSH and its copper(II) complexes was accomplished by elemental analysis, electronic, infrared (IR), mass, proton nuclear magnetic resonance (¹H NMR), electron spin resonance spectra, thermal analysis, molar conductivity, and magnetic susceptibility measurements. The density functional theory (DFT) at 6-311G (d,p) level was used to calculate the structural parameters of the optimized structures of the prepared compounds. FCSH and its copper(II) complexes showed antitumor activity towards HepG2 cell line. The docking study of FCSH ligand and its complexes showed that the ligand and its complexes have a strong binding propensity to CDK2 proteins.

2 | EXPERIMENTAL

2.1 | Materials

Following the literature method, salicylaldehyde hydrazone^[16] and 3-formylchromone^[17] were synthesized. Copper(II) salts (Cu (OAc)₂·H₂O, Cu (NO₃)₂·3H₂O, CuSO₄·5H₂O, Cu (ClO₄)₂·6H₂O, CuCl₂·2H₂O, and CuBr₂), Na₂EDTA, and murexide were Merck, BDH, or Aldrich products. Organic solvents were reagent grade chemicals and were used as received. Human Hepatocellular carcinomas (HepG-2 cells) were attained from VACSERA Tissue Culture Unit. HEPES buffer solution, fetal bovine

serum, L-glutamine, gentamycin, DMEM, RPMI-1640, and Trypsin-EDTA (0.25%) were obtained from Lonza. Trypan blue dye and crystal violet were obtained from Sigma.

2.2 | Measurements

Microanalyses of C, H, N, and S were performed at the Micro-analytical Center, Cairo University, Egypt. A digital Stuart SMP3 melting point apparatus was utilized to determine melting points (decomposition temperatures) of the synthesized compounds. Copper(II) ion was estimated by EDTA complexometrically after decomposition of the complexes with conc. HNO₃. Fourier-transform IR (FTIR) Nicolet IS10 spectrometer was employed to record the IR spectra (as KBr discs). A Bruker WP 200 SY spectrometer was employed to record proton NMR of FCSH ligand at room temperature. The solvent was dimethyl sulfoxide, DMSO-*d*₆, and the internal reference was tetramethylsilane. A Jasco V-550 UV/Vis spectrophotometer was utilized to record electronic spectra. Measurements were carried out as solutions in dimethylformamide and/or Nujol mulls. An Elexsys (E500), Bruker company, was utilized to record electron spin resonance spectra of the complexes. DPPH; 2,2'-diphenyl-1-picrylhydrazyl was utilized to calibrate the magnetic field. A gas chromatographic GCMSqp 1000 Ex Shimadzu instrument was employed to record mass spectra. A Shimadzu-50 thermal analyzer was employed for measurements of thermal gravimetric analysis under nitrogen (at a heating rate of 10°C/min). A corning conductivity meter NY 14831 (model 441) was employed for molar conductivities measurements (concentration = 1 × 10⁻³ M in dimethylformamide). A Johnson Matthey magnetic susceptibility balance (Alfa product) Model No. MKI was employed for magnetic susceptibility measurements at room temperature. Pascal's constants for the diamagnetism of all atoms that exist in the complexes^[18] were used to correct the calculated effective magnetic moments.

2.3 | Synthesis of FCSH ligand

FCSH ligand (Figure 1) was synthesized by adding salicylaldehyde hydrazone (1.95 g, 14.32 mmol) in

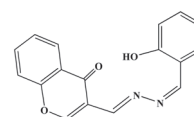


FIGURE 1 Structure of the hydrazone ligand

absolute ethanol (~25 ml) to 3-formylchromone (2.5 g, 14.36 mmol) in absolute ethanol (~30 ml). The reaction mixture was stirred for 2 h. The product was collected, filtered off, and washed with ethanol then diethylether and recrystallized from ethanol (yield = 76%).

2.4 | Synthesis of the metal complexes

To FCSH in ethanol, copper(II) salt was added in the molar ratio 1:1 (FCSH:M) and heated under reflux for 6 h. In case of acetate anion, 1:2 (FCSH:M) molar ratio was also carried out. The resultant precipitates were collected by filtration, washed with ethanol then ether, and dried over CaCl_2 .

2.5 | Computational method

DFT calculations were carried out for FCSH and its complexes using *Gaussian 09* program package.^[19] Gauss View 5.0 package was employed to get various graphic views of molecular charges and shapes of distinctive molecular orbitals.

2.6 | Biological activity

2.6.1 | Antitumor activity

Antitumor activity of FCSH and its complexes was checked on HepG2 cells by determining the effect of the test samples on cell morphology and cell viability following literature protocol.^[20,21]

2.6.2 | Molecular docking study

All the molecular modeling studies were carried out using Molecular Operating Environment (MOE, 2015.10) software. All minimizations were performed with MOE until a root mean square deviation (RMSD) gradient of $0.05 \text{ kcal mol}^{-1} \text{ \AA}^{-1}$ with MMFF94x force field and the partial charges were automatically calculated.

The X-ray crystallographic structure of CDK-2 enzyme (PDB ID: 3IG7) was downloaded from the protein data bank.^[22] For the co-crystallized enzyme, water molecules and ligands that are not involved in the binding were eliminated; the protein was prepared for the docking study by means of *Protonate 3D* protocol in MOE with default options. Triangle Matcher placement method and London dG scoring function were utilized in docking. FCSH and its Cu(II) complexes were then

docked within the active site of the crystallized structure using the MOE dock tool in MOE, performed with the default values. The active site was defined by all the amino acid residues involved in the interaction with the co-crystallized ligand (inhibitors).

3 | RESULTS AND DISCUSSION

3.1 | The HL

The important analytical and physical data of FCSH and its Cu(II) complexes are summarized in Table 1.

Table 2 lists the ^1H NMR spectral data of FCSH relative to TMS in $\text{DMSO-}d_6$, and Figure 2 depicts the spectra. The signal observed at 11.07 ppm may be due to the OH proton. The specific singlet signals of the two azomethine protons ($2\text{CH}=\text{N}$) are observed at δ 8.92 and 8.99 ppm. The signal characteristic to H-2 of the chromone nucleus ($\text{H-2}_{\text{chromone}}$) appeared at δ 8.77 ppm. Finally, the signals due to aromatic protons are detected in the range δ 6.96–8.16 ppm.

Table 3 lists the main IR spectral data of FCSH and its copper(II) complexes. The IR spectrum of FCSH displayed four clear bands at 3,424, 1,629, 1,613, and $1,270 \text{ cm}^{-1}$, which may be related to ν (OH), $\nu(\text{C}=\text{O})_{\gamma\text{-pyrone}}$, $\nu(\text{C}=\text{N})$, and $\nu(\text{C}-\text{O})$ phenolic, respectively.^[16,23,24]

Table 4 lists the electronic spectral data of FCSH and its copper(II) complexes in dimethylformamide. The spectrum of FCSH displayed three bands at 280, 307, and 345 nm. The higher energy band may be related to π - π^* transitions of the chromone ring, azomethine linkage, and the aromatic benzene ring. The second energy band may be due to charge transfer transitions regarding the whole molecule as well as π - π^* transitions including the chromone and phenyl rings and/or azomethine groups. The lower energy band may be due to the n - π^* transitions of the azomethine group.

Figure 3 depicts the mass spectrum of FCSH. The spectrum displayed the molecular ion peak at m/z 292.29, verifying its formula weight (F. Wt = 292.30).

3.2 | Metal complexes

Reactions of FCSH with different copper(II) salts (acetate, nitrate, sulfate, perchlorate, chloride, and bromide) yielded seven stable and non-hygroscopic complexes. The prepared complexes are characterized by elemental analysis, electronic, IR, mass, electron spin resonance spectra, thermal analysis, molar conductivity, and magnetic susceptibility measurements. Elemental

TABLE 1 Analytical and physical data of the hydrazone ligand and its complexes

No.	Reaction	Complex M. F. [F. Wt]	Color	Yield (%)	M.P. (°C)	Elemental analysis, % found/(calc.)				
						C	H	N	Cl/Br/S	M
	HL	C ₁₇ H ₁₂ N ₂ O ₃ [292.30]	Yellow	76	240	69.86 (69.86)	4.28 (4.14)	9.45 (9.58)	—	—
(1)	HL + Cu (OAc) ₂ . H ₂ O (1:1)	[Cu(L)(OAc)(H ₂ O) ₂].0.5H ₂ O C ₁₉ H ₁₉ N ₂ O _{7.5} Cu [458.92]	Brown	69	253	50.33 (49.73)	3.72 (4.17)	6.40 (6.10)	—	14.00 (13.85)
(2)	HL + Cu (OAc) ₂ . H ₂ O (1:2)	[Cu ₂ (L)(OAc) ₃ (H ₂ O) ₅].H ₂ O C ₂₃ H ₃₂ N ₂ O ₁₅ Cu ₂ [703.61]	Brown	52	259	39.70 (39.26)	4.30 (4.58)	4.20 (3.98)	—	17.80 (18.06)
(3)	HL + Cu (NO ₃) ₂ .3H ₂ O	[Cu(L)(NO ₃)(EtOH)(H ₂ O)] ₂ .0.5H ₂ O C ₁₉ H ₂₀ N ₃ O _{8.5} Cu [489.93]	Brown	68	>300	46.25 (46.58)	3.8 (4.11)	8.80 (8.58)	—	12.60 (12.97)
(4)	HL + CuSO ₄ .5H ₂ O	[Cu (HL)(SO ₄)(H ₂ O) ₂].2H ₂ O C ₁₇ H ₂₀ N ₂ O ₁₁ SCu [523.97]	Reddish brown	56	>300	38.60 (38.97)	3.60 (3.85)	5.60 (5.35)	5.90 (6.12)	11.80 (12.13)
(5)	HL + Cu (ClO ₄) ₂ .6H ₂ O	[Cu(L)(ClO ₄)(EtOH) ₂] C ₂₁ H ₂₃ N ₂ O ₉ ClCu [546.42]	Brown	63	^a	46.30 (46.16)	3.90 (4.24)	5.50 (5.13)	^a (6.49)	^a (11.63)
(6)	HL + CuCl ₂ .2H ₂ O	[Cu(L)Cl (EtOH)(H ₂ O)] C ₁₉ H ₁₉ N ₂ O ₅ ClCu [454.37]	Brown	66	253	50.60 (50.23)	3.80 (4.21)	6.60 (6.17)	^a (7.80)	13.70 (13.99)
(7)	HL + CuBr ₂ (Stirring)	[Cu(L)Br (EtOH) ₂].H ₂ O C ₂₁ H ₂₅ N ₂ O ₆ BrCu [544.89]	Brown	70	260	45.99 (46.29)	4.20 (4.62)	5.10 (5.14)	^a (14.66)	11.40 (11.66)

^aNot determined.

TABLE 2 ^1H nuclear magnetic resonance (NMR) spectral data of the hydrazone ligand

Chemical shifts in ppm (DMSO)	Assignment
6.961–8.16	(m, 8H, Ar–H)
8.77	(s, 1H, (C ₂ –H) _{chromone})
8.92, 8.99	(s, 2H, 2-CH=N)
11.07	(s, 1H, OH, exchangeable with D ₂ O)

Abbreviation: DMSO, dimethyl sulfoxide.

analyses data (Table 1) showed the formation of 1:1 and 1:2; FCSH:Cu complexes.

3.2.1 | IR spectra

Table 3 lists the main IR spectral data of the complexes. In all complexes, the broad bands observed in the range 3,409–3,563 cm^{-1} may be due to ν (OH) of the non-coordinated or coordinated water and/or ethanol

molecules connected to the complexes. The bands at 1,629 and 1,613 cm^{-1} ascribed to $\nu(\text{C}=\text{O})_{\gamma\text{-pyrone}}$ and $\nu(\text{C}=\text{N})$, respectively, in the uncomplexed FCSH were shifted to lower wave number in the complexes, demonstrating the contribution of these groups in complex-formation.^[25] As the stretching frequency of $\nu(\text{C}=\text{O})$ is shifted to lower wave number ($\Delta\nu_{\text{C}=\text{O}}$), the extent of interaction with the Cu(II) ion increases (high stability of complex formation that respective to E_{gap} , *vide infra*). This interpretation is emphasized by the positive slope of the linear relationship of (E_{gap}) versus ($\Delta\nu_{\text{C}=\text{O}}$), $E_{\text{gap}}/\text{eV} = -20.462 + 0.889\Delta\nu_{\text{C}=\text{O}} \text{ cm}^{-1}$, $r = 0.87$ ($n = 5$ points, except CuSO_4 and CuCl_2 complexes). Moreover, the negative slope of $\nu\text{M-O}$ versus $\text{C}=\text{N}$, $\nu\text{M-O}/\text{cm}^{-1} = 20.336 - 12.605 \nu\text{C}=\text{N}/\text{cm}^{-1}$, $r = 0.98$, $n = 5$, except $\text{Cu}(\text{OAc})_2$, $\text{Cu}(\text{ClO}_4)_2$, reveals that the strong interaction of $\text{C}=\text{O}$ with copper(II) was accompanied by high extent of back donation to the azomethine group that enhances its interaction with copper ion (shift to a lower frequency). Further evidence, $\text{M-N}/\text{cm}^{-1} = 416.83 + 0.694 \Delta\nu_{\text{C}=\text{O}}/\text{cm}^{-1}$, $r = 0.87$, $n = 4$, except $\text{Cu}(\text{NO}_3)_2$, CuCl_2 , and CuBr_2 complexes, the positive slope reveals that the strong M–N bond

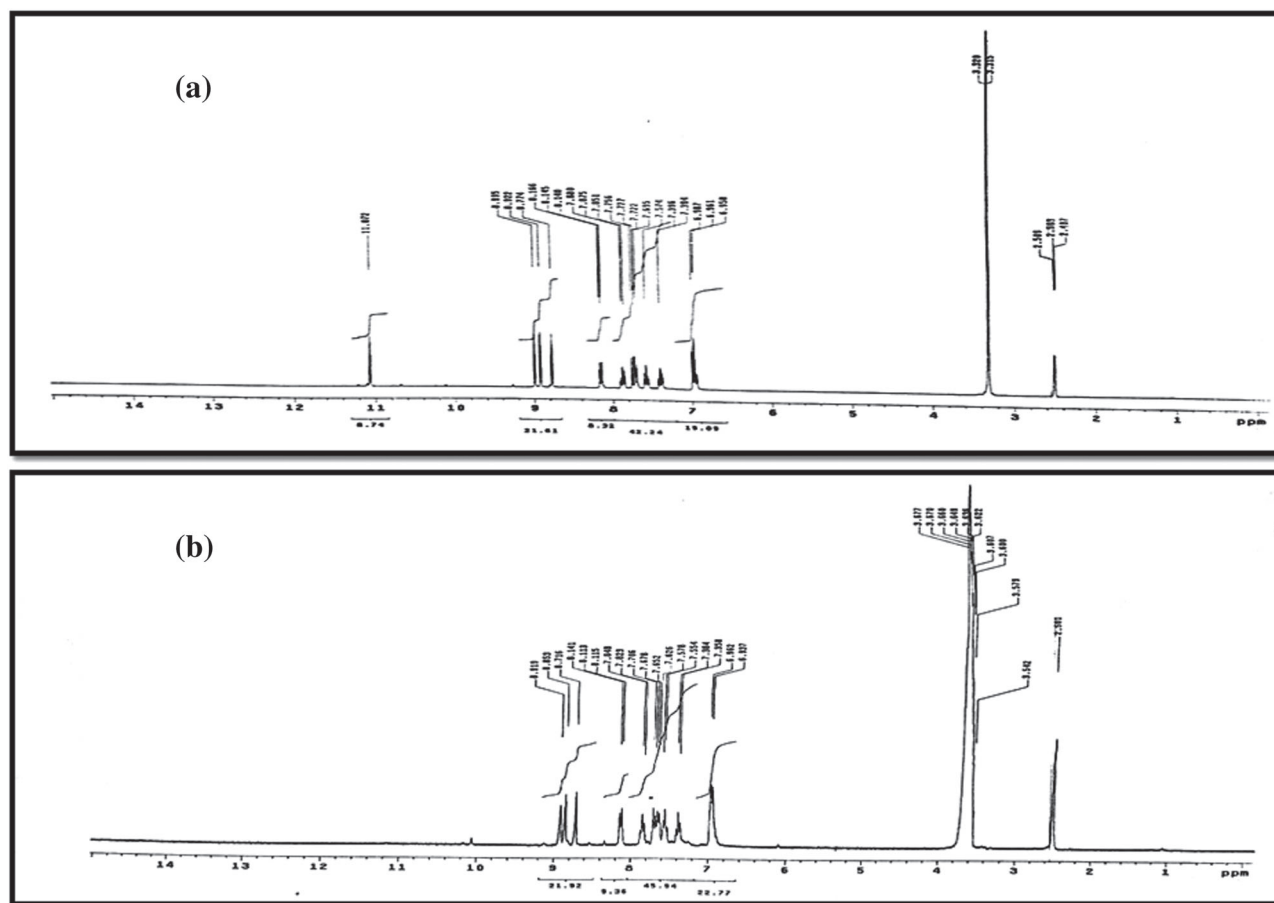
**FIGURE 2** ^1H NMR spectrum (δ ppm) of the hydrazone ligand (a) in dimethyl sulfoxide (DMSO) and (b) after addition of D₂O

TABLE 3 Characteristic infrared (IR) spectral data of the hydrazone ligand and its complexes

No.	Complex	IR spectra (cm ⁻¹)						
		ν (OH)	ν (C=O)	ν (C=N)	ν (C-O) Phenolic	ν (M-O)	ν (M-N)	Other bands
	HL	3,424	1,629	1,613	1,270	—	—	—
1	[Cu(L)(OAc)(H ₂ O) ₂].0.5H ₂ O	3,563	1,602	1,578	1,279	502	432	1,485, $\nu_{as}(\text{COO}^-)$; 1,229, $\nu_s(\text{COO}^-)$; (monodentate OAc ⁻)
2	[Cu ₂ (L)(OAc) ₃ (H ₂ O) ₅].H ₂ O	3,420	1,605	1,568	1,287	545	438	1,477, $\nu_{as}(\text{COO}^-)$; 1,229, $\nu_s(\text{COO}^-)$; (monodentate OAc ⁻)
3	[Cu(L)(NO ₃)(EtOH)(H ₂ O)].0.5H ₂ O	3,445	1,603	1,570	1,282	593	424	1,385, 833; ν (NO ₃ ⁻) (monodentate)
4	[Cu (HL)(SO ₄)(H ₂ O) ₂].2H ₂ O	3,419	1,617	1,570	1,279	560	424	1,112, 1,068; ν (SO ₄ ²⁻) (monodentate)
5	[Cu(L)(ClO ₄)(EtOH) ₂]	3,419	1,619	1,605	1,278	515	424	1,136, 1,063, 969; ν (ClO ₄ ⁻) (monodentate)
6	[Cu(L)Cl (EtOH)(H ₂ O)]	3,446	1,603	1,568	1,278	500	410	—
7	[Cu(L)Br (EtOH) ₂].H ₂ O	3,409	1,604	1,570	1,275	590	424	—

TABLE 4 Electronic spectra, magnetic moments, and molar conductivity data of the hydrazone ligand and its complexes

No.	Complex	Electronic spectral bands ^a (nm)	$\mu_{\text{eff.}}^{\text{d}}$ B.M.	$\mu_{\text{eff.}}^{\text{f}}$ B.M.	Conductance ^a ($\Omega^{-1} \text{ cm}^2 \text{ mol}^{-1}$)
		$\lambda_{\text{max}}^{\text{a}}$ (nm)/($\epsilon_{\text{max}} \text{ L cm}^{-1} \text{ mol}^{-1}$)			
	HL	(280, 307, 345) ^a	—	—	—
1	[Cu(L)(OAc)(H ₂ O) ₂].0.5H ₂ O	(287, 402) ^a (672) ^c (434, 709) ^b	1.80	1.84	4.62
2	[Cu ₂ (L)(OAc) ₃ (H ₂ O) ₅].H ₂ O	(414) ^a (666) ^c (404, 683, 710) ^b	1.81, (2.56) ^e	1.81	9.59
3	[Cu(L)(NO ₃)(EtOH)(H ₂ O)].0.5H ₂ O	(560) ^a (680) ^c (694) ^b	1.8	1.85	31.84
4	[Cu (HL)(SO ₄ (H ₂ O) ₂].2H ₂ O	(321, 438) ^a (665) ^c (713) ^b	1.97	1.88	14.02
5	[Cu(L)(ClO ₄)(EtOH) ₂]	(291, 332, 419, 665) ^a (484, 687) ^b	2.40	1.81	25.16
6	[Cu(L)Cl (EtOH)(H ₂ O)]	(287, 401) ^a (471, 706) ^b	1.72	1.84	13.47
7	[Cu(L)Br (EtOH) ₂].H ₂ O	(295, 342, 456, 674) ^a (653) ^c (404, 710) ^b	2.03	—	29.92

^aSolutions in dimethylformamide (DMF) (10⁻³ M).^bNujol mull.^cConcentrated solutions.^d $\mu_{\text{eff.}}$ is the magnetic moment of one cationic species in the complex.^e $\mu_{\text{compl.}}$ is the total magnetic moments of all cations in the complex.^f $\mu_{\text{eff.}}$ is the magnetic moment calculated from electron spin resonance (ESR) spectral data.

accompanied by higher shift of C=O to a lower frequency. However, the band ascribed to ν (C-O) phenolic was shifted to higher wave number in the complexes, indicating chelation *via* deprotonated phenolic OH group.^[26,27] In acetato complexes (**1** and **2**), the new bands detected at 1485 and 1,229 cm⁻¹ for **1** and at 1477 and 1,229 cm⁻¹ for **2** may be due to ν_{as} (COO⁻) and ν_s

(COO⁻) of the acetate group, respectively.^[28] As the difference between the two bands in **1** and **2**; ($\Delta\nu = \nu_{as} - \nu_s$) is equal to 256 and 248 cm⁻¹, respectively, that is, higher than 200 cm⁻¹, a monodentate nature of the acetate anion was suggested.^[29] The nitrate complex **3** displayed new bands at 1,384 and 833 cm⁻¹, demonstrating the monodentate nature of the nitrate group.^[30] In sulphato

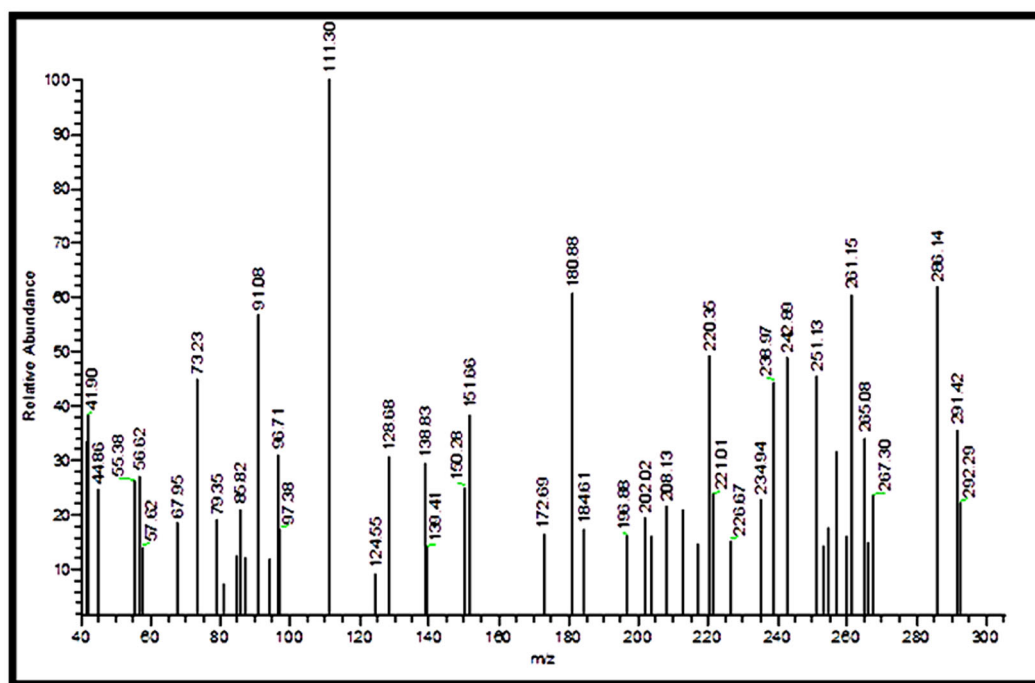


FIGURE 3 Mass spectrum of the hydrazone ligand

complex **4**, the new bands detected at 1,112 and 1,068 cm^{-1} may be attributed to the sulfate group in a monodentate fashion.^[31] The perchlorato complex **5** exhibited three new bands observed at 1,136, 1,063 (ν_3), and 969 (ν_6) cm^{-1} , which may be ascribed to the monodentate perchlorate group.^[32,33] At last, the previous interpretation is confirmed by new bands at 500–593 and 410–438 cm^{-1} , which may be due to ν (Cu–O) and ν (Cu–N), respectively.^[34,35]

3.2.2 | Conductivity measurements

Table 4 lists the molar conductance values of copper-FCSH complexes in dimethylformamide. The results illustrated the non-electrolytic nature of all complexes.^[36]

3.2.3 | Magnetic moment measurements and electronic spectra

The calculated magnetic moment values of copper-FCSH complexes (Table 4) are in the range 1.72–2.03 B.M., which is compatible with the presence of an unpaired electron in d^9 -system, excluding the presence of antiferromagnetic interaction.^[37,38] The spin–orbit coupling may be the reason for the higher magnetic moment value (2.4 B.M.) given by the perchlorato complex **5**.^[39] In the binuclear copper(II) complex **2**, the low value of

magnetic moment ($\mu_{\text{compl}} = 2.56$ B.M.) may be due to a weak coupling of the unpaired electrons, one on each Cu(II) ion.

The electronic spectra of copper-FCSH complexes exhibited absorption bands in the range 560–713 nm, which may be attributed to the ${}^2E_g \rightarrow {}^2T_{2g}$ transition in a distorted octahedral geometry.^[40,41] Some complexes (Table 4) exhibited another band (within the range 401–456 nm), which may be caused by charge transfer.^[38] It was found that the complexes retain its stability and integrity in the solution where the profile of the spectra and positions of the bands are nearly the same as that recorded as Nujol mulls. This reflects the irrelevant effect of dimethylformamide on the complex configuration.

3.2.4 | Electron spin resonance spectra

The electron spin resonance spectra of copper-FCSH complexes (**1–6**)—as solid samples—were recorded. As representative complexes, the spectra of the acetato **2** and sulphato **4** complexes are depicted in Figure 4. The spectra of the complexes (**1**, **3**, and **6**) exhibit two signals with two g values while the complexes (**2**, **4**, and **5**) show rhombic symmetry with three g values (Table 5). The shapes of the spectra revealed octahedral geometry for the prepared complexes.^[42,43] Table 5 lists the calculated spin Hamiltonian parameters of the copper-FCSH complexes. The spectra of the complexes exhibit an

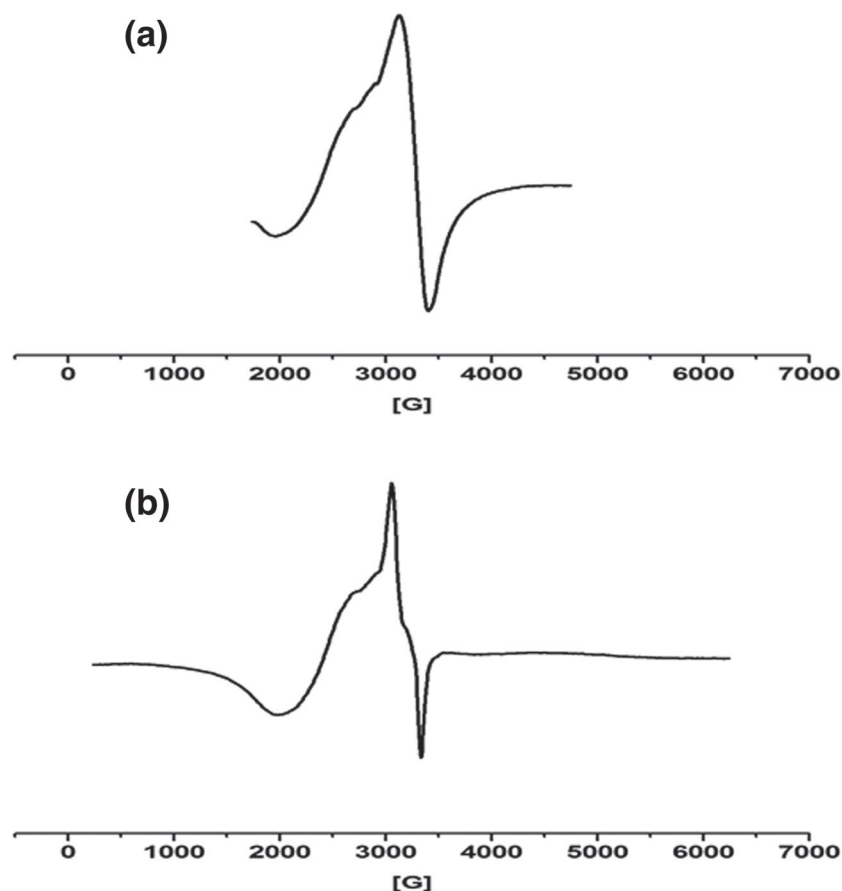


FIGURE 4 X-band electron spin resonance (ESR) spectra of the complexes (a) $[\text{Cu}_2(\text{L})(\text{OAc})_3(\text{H}_2\text{O})_5] \cdot \text{H}_2\text{O}$ (**2**) and (b) $[\text{Cu}(\text{HL})(\text{SO}_4)(\text{H}_2\text{O})_2] \cdot 2\text{H}_2\text{O}$ (**4**)

TABLE 5 Electron spin resonance (ESR) data of some copper(II) complexes at room temperature

Complex	g_1	g_2	g_3	g_{\parallel}	g_{\perp}	$A_{\parallel} \times 10^{-4} \text{ (cm}^{-1}\text{)}$	R	G	α^2	β^2	γ^2	K_{\parallel}	K_{\perp}
$[\text{Cu}(\text{L})(\text{OAc})(\text{H}_2\text{O})_2] \cdot 0.5\text{H}_2\text{O}$ (1)				2.23	2.09	205		2.6	0.87	0.59	0.91	0.72	0.89
$[\text{Cu}_2(\text{L})(\text{OAc})_3(\text{H}_2\text{O})_5] \cdot \text{H}_2\text{O}$ (2)	2.18	2.07	2.01				0.61						
$[\text{Cu}(\text{L})(\text{NO}_3)(\text{EtOH})(\text{H}_2\text{O})] \cdot 0.5\text{H}_2\text{O}$ (3)				2.26	2.08	226		3.3	0.96	0.6	0.72	0.76	0.83
$[\text{Cu}(\text{HL})(\text{SO}_4)(\text{H}_2\text{O})_2] \cdot 2\text{H}_2\text{O}$ (4)	2.28	2.16	2.07				0.72						
$[\text{Cu}(\text{L})(\text{ClO}_4)(\text{EtOH})_2]$ (5)	2.19	2.08	2.01				0.60						
$[\text{Cu}(\text{L})\text{Cl}(\text{EtOH})(\text{H}_2\text{O})]$ (6)				2.19	2.1	227		1.9	0.9	0.45	0.93	0.63	0.91

axially g -tensor parameters with $g_{\parallel} > g_{\perp} > 2.0023$. The g_{\parallel} value is an important function for demonstrating covalent character of metal–ligand bonds^[44] (g_{\parallel} is higher than 2.3 for ionic character, and g_{\parallel} is lower than 2.3 for covalent character). Based on g_{\parallel} values (see Table 5), a covalent character for the Cu-FCSH bond was indicated. In addition, the exchange interaction parameter term G was calculated by the relation; $G = (g_{\parallel} - 2)/(g_{\perp} - 2)$.^[45,46] As G values are lower than four, copper–copper exchange interactions were indicated.

The electron spin resonance (ESR) spectra of the complexes **2**, **4**, and **5** are characterized by three g values. Commonly, the higher value is indicated as g_1 and lower as g_3 . This suggests that the ground state is a combination of the dz^2 and dx^2-y^2 orbitals. For complexes of this type, a parameter $R = (g_2 - g_1)/(g_3 - g_2)$ can be indicative of the predominance of the dz^2 or dx^2-y^2 orbital in the ground state, with $g_1 > g_2 > g_3$. If $R > 1$, the greater contribution to the ground state arises from dz^2 orbital; if $R < 1$, the greater contribution to the ground state arises

from dx^2-y^2 orbital. The present complexes have values $R < 1$, suggesting distorted octahedral geometry with a dx^2-y^2 ground state.^[47] Magnetic moment values are also calculated from ESR technique by the following relation, $\mu_{\text{soc}} = [g^2 s(s + 1)]^{0.5}$, where “s” is theoretical value of the spin. The calculated values are in the range 1.81–1.88 B.M., which agree well with the experimental data for all complexes except complex 5.

Furthermore, molecular orbital coefficients, α^2 (a quantity of the covalency of the in-plane σ -bonding between copper 3d orbital and FCSH orbitals), β^2 (covalent in-plane π -bonding), and γ^2 (covalent out-of plane π -bonding) were successfully computed.^[48] β^2 values are smaller than those of α^2 demonstrating that the in-plane π -bonding is more covalent than the in-plane σ -bonding. The observed values of γ^2 indicate that there is substantial interaction in the out-of-plane π -bonding.^[40,49] This is also confirmed by the orbital reduction factors, $K_{\parallel} = \alpha^2 \beta^2$ and $K_{\perp} = \alpha^2 \gamma^2$, which were calculated using the following expressions:

$$K_{\parallel}^2 = (g_{\parallel} - 2.0023)E_{d-d}/8\lambda_0, \quad K_{\perp}^2 = (g_{\perp} - 2.0023)E_{d-d}/2\lambda_0,$$

Where λ_0 is the spin-orbit coupling constant, with a value of -828 cm^{-1} for a copper(II) d^9 -system. According to Hathaway,^[45] for pure σ -bonding, $K_{\parallel} \approx K_{\perp} \approx 0.77$, and for in-plane π -bonding $K_{\parallel} < K_{\perp}$; while for out-of-plane π -bonding, $K_{\perp} < K_{\parallel}$. In the present complexes, it is observed that $K_{\parallel} < K_{\perp}$, indicating the presence of significant in-plane π -bonding.

3.2.5 | Thermal analysis

The nature of water or solvent molecules (which are linked to the complex) can be judged by thermal

gravimetric analysis. This technique helps researchers to decide the nature of linked molecules to be within the internal or external coordination sphere of the metal ion.^[50] In the present work, complexes 1–4 and 7 were selected for thermal analysis and the results are listed in Table 6. Figure 5 depicts the thermograms of complexes 4 and 7 as representative examples.

The thermogram of the mononuclear acetato complex 1 displayed two degradation steps within the temperature range 40–298°C, which may be due to loss of half non-coordinated water molecule for the first stage and two coordinated water, one AcOH, and two C_2H_2 molecules for the second step (weight loss; calc./found%; 1.96/1.54 and 32.25/32.42%, respectively). However, the thermogram of the binuclear acetato complex 2 displayed two weight losses steps in the ranges 40–129°C and 130–270°C, which may be related to the loss of one non-coordinated water molecule and five coordinated water in addition to 3AcOH molecules, respectively (weight loss; calc./found%; 2.56/2.34 and 38.37/38.28%, respectively).

The nitrate complex 3 exhibited two degradation steps in the ranges 32–100°C and 101–308°C, which may be due to loss of half non-coordinated water molecule for the first step and one coordinated water, one coordinated ethanol, one NO_2 , and one C_2H_2 molecules for the second step (weight loss; calc./found%; 1.84/2.3 and 27.76/27.7%, respectively).

The thermogram of the sulphato complex 4 displayed two degradation steps in the ranges 39–159°C and 160–270°C, which may be due to loss of two non-coordinated water molecules and two coordinated water in addition to one SO_2 molecules, respectively (weight loss; calc./found%; 6.87/6.10 and 19.09/19.4%, respectively).

TABLE 6 Thermal analysis data of some metal complexes

Complex	Temperature range (°C)	% Wt. loss found/(calc.)	Lost fragment (no. of molecules)
[Cu(L)(OAc)(H ₂ O) ₂].0.5H ₂ O (1)	40–156	1.54/(1.96)	0.5 H ₂ O (solv.)
	157–298	32.42/(32.25)	2 H ₂ O (coord.) + 1 AcOH + 2 CH \equiv CH
[Cu ₂ (L)(OAc) ₃ (H ₂ O) ₅].H ₂ O (2)	40–129	2.34/(2.56)	1 H ₂ O (solv.)
	130–270	38.28/(38.37)	+5 H ₂ O (coord.) + 3 AcOH
[Cu(L)(NO ₃)(EtOH)(H ₂ O)].0.5H ₂ O (3)	32–100	2.3/(1.84)	0.5 H ₂ O (solv.)
	101–308	27.7/(27.76)	1 EtOH (coord.) + 1 H ₂ O (coord.) + 1 NO ₂ + 1 CH \equiv CH
[Cu (HL)(SO ₄)(H ₂ O) ₂].2H ₂ O (4)	39–159	6.10/(6.87)	2 H ₂ O (solv.)
	160–270	19.4/(19.09)	2 H ₂ O (coord.) + 1 SO ₂
[Cu(L)Br (EtOH) ₂].H ₂ O (7)	28–127	3.12/(3.3)	1 H ₂ O (solv.)
	128–250	16.82/(16.88)	2 EtOH (coord.)

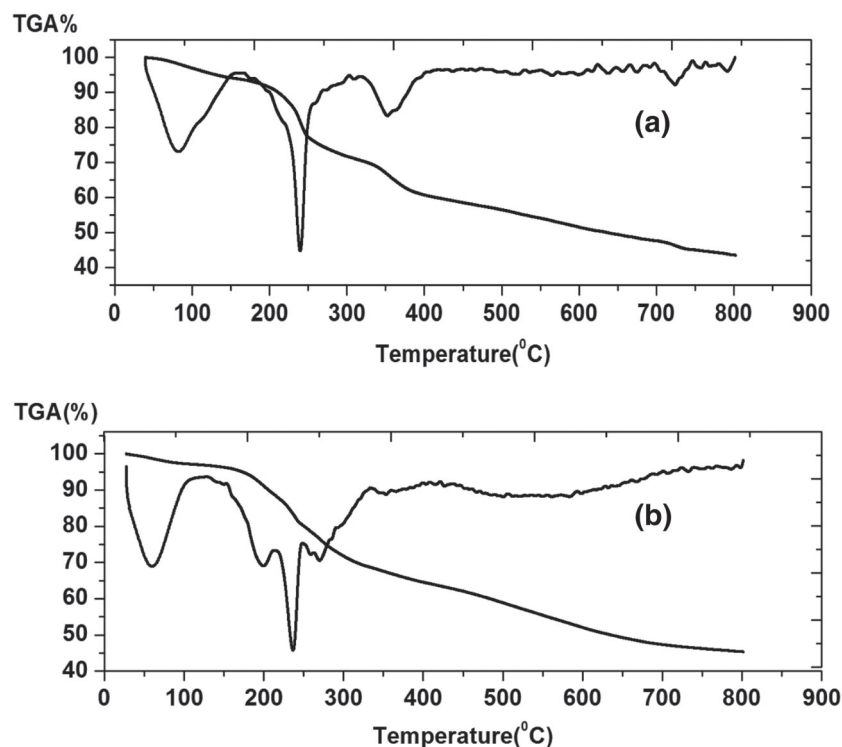


FIGURE 5 Thermograms of the complexes (a) [Cu (HL)(SO₄)(H₂O)₂].2H₂O and (b) [Cu(L) Br (EtOH)₂].H₂O

Finally, the thermogram of the bromo complex **7** displayed two decomposition steps in the ranges 28–127°C and 128–250°C, which may be due to loss of one non-coordinated water and two coordinated ethanol molecules, respectively (weight loss; calc./found%; 3.3/3.12 and 16.88/16.82%, respectively).

In addition, the order n and the activation parameters of the various degradation steps of copper-FCSH complexes were determined from the TG thermograms using the Coats–Redfern equations,^[51] and the kinetic parameters are summarized in Table 7. The following points can

be concluded: (a) As ΔH values are +ve, the decomposition processes are endothermic. (b) Since the energy of activation values E for the second stage of degradation of complexes **1–3** are lower than the first stage, the rate of decomposition for this stage is higher than that of the first stage. In case of complexes **4** and **7**, the second step of decomposition is higher than the first step. This confirms that the rate of decomposition for this stage is lower in the second step.^[52] (c) As ΔS values for complexes are –ve, the activated complex is more ordered than the reactants and/or the reactions are slow.^[53] (d) ΔG values are

TABLE 7 Temperatures of decomposition and the kinetic parameters of complexes

Compound	Step	n Order	T (K)	A (S ⁻¹)	ΔE (kJ mol ⁻¹)	ΔH (kJ mol ⁻¹)	ΔS (kJ mol ⁻¹ K ⁻¹)	ΔG (kJ mol ⁻¹)
[Cu(L)(OAc)(H ₂ O) ₂].0.5H ₂ O (1)	First	1	331	2.80×10^7	14.52	11.77	-0.112	48.68
	Second	1	520	1.8×10^3	0.838	-3.48	-0.195	97.83
[Cu ₂ (L)(OAc) ₃ (H ₂ O) ₅].H ₂ O (2)	First	0.66	370	9.1899	541.08	38.01	-0.237	125.5
	Second	0	517	1.95×10^2	37.88	33.58	-0.214	144.32
[Cu(L)(NO ₃)(EtOH)(H ₂ O)].0.5H ₂ O (3)	First	1	337	2.11×10^6	44.02	41.22	-0.133	86.12
	Second	0	415	1.03×10^9	9.49	6.04	-0.084	40.81
[Cu (HL)(SO ₄)(H ₂ O) ₂].2H ₂ O (4)	First	1	355	8.05×10^4	36.15	33.20	-0.161	90.28
	second	0.33	513	1.28×10^6	39.91	35.65	-0.141	107.95
[Cu(L)Br (EtOH) ₂].H ₂ O (7)	First	1	333	2.49×10^3	2.03	-0.74	-0.189	62.33
	Second	0	510	2.03×10^7	26.22	21.98	-0.118	82.07

comparatively low and of +ve sign, demonstrating the autocatalytic action of metal ions on thermal degradation of the complexes and non-spontaneous processes.^[54]

3.2.6 | Mass spectra

The mass spectra of the investigated copper-FCSH complexes **1–4** and **7**, as representative examples, were recorded. Figures 6–8 depict the mass spectra of complexes **1**, **2**, and **4**. The mass spectra of the complexes **1–4** and **7** displayed the molecular ion peaks with m/z 449, 685, 481, 488, and 526, respectively, which are consistent with their anhydrous formula weights [(L)Cu(OAc)(H₂O)₂]; (F. Wt = 449.92), [(L)Cu₂(OAc)₃(H₂O)₅]; (F. Wt = 685.57), [(L)Cu(NO₃)(EtOH)(H₂O)]; (F. Wt = 480.91), [(L)Cu(SO₄)(H₂O)₂]; (F. Wt = 487.93), and [(L)CuBr(EtOH)₂]; (F. Wt = 526.87), respectively.

With the aid of the forgoing results of analytical and spectral methods, Figure 9 represents the suggested structures of copper-FCSH complexes.

3.3 | Molecular orbital calculations

The molecular geometry for FCSH ligand (HL) and its copper complexes was fully optimized by DFT at B3LYP/6-311G (p,d) by the *Gaussian 09* program in the gas phase.^[55] The geometrical structures, highest

occupied molecular orbital (HOMO) and lowest unoccupied molecular orbital (LUMO) of FCSH ligand and complex **1** were shown in Figures 10–13. The calculated structure parameters of FCSH ligand and its complexes are tabulated in Table 8. Molecular parameters and chemical quantum factors including absolute electronegativity (χ), absolute hardness (η), absolute softness (σ), global softness (S), chemical potential (π), global electrophilicity (ω), and additional electronic charge (ΔN_{\max}) were evaluated such as reported.^[56–58]

The HOMO–LUMO energy gap, E_{gap} , which is an important stability index, is applied to develop theoretical models for explaining the structure and conformation barriers in many molecular systems.^[59] The energies of the LUMO and HOMO are of negative values, showing the stability of isolated complexes.^[60] Correlations of frontier orbitals data in Table 8 versus the experimental data supported the assignments given above. Linear correlation between (E_{LUMO}) versus the stretching frequency of the C=O group ($\nu_{\text{C=O}}$), $E_{\text{LUMO}}/\text{eV} = -14.375 + 0.43846 \Delta\nu_{\text{C=O}}/\text{cm}^{-1}$, $r = 0.895$ ($n = 5$ points, except complexes **4** and **5**). The positive slope of the linear relationship reveals that the increase in E_{LUMO} was accompanied by a higher shift of the stretching frequency of the $\nu_{\text{C=O}}$ to a lower wave number.

The chemical reactivity and stability of each nominated molecule depend on the eigen values of HOMO–LUMO and energy gaps. The energy gap (E_{gap}) of the studied complexes varied between 0.436 for complex **2**,

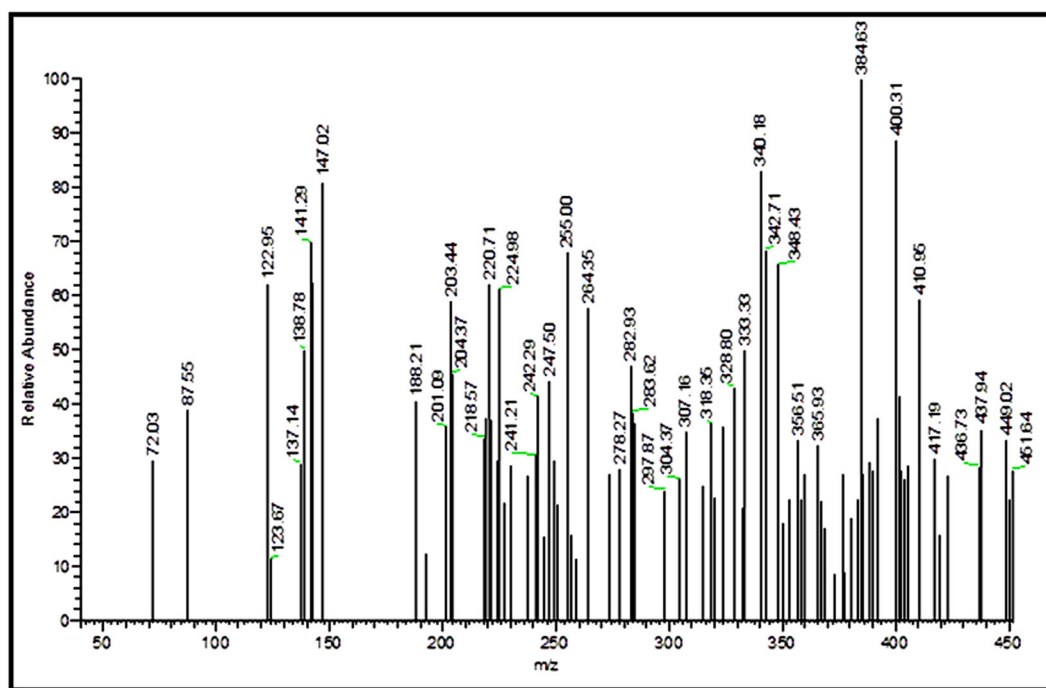


FIGURE 6 Mass spectrum of complex **1**; [Cu(L)(OAc)(H₂O)₂].0.5H₂O

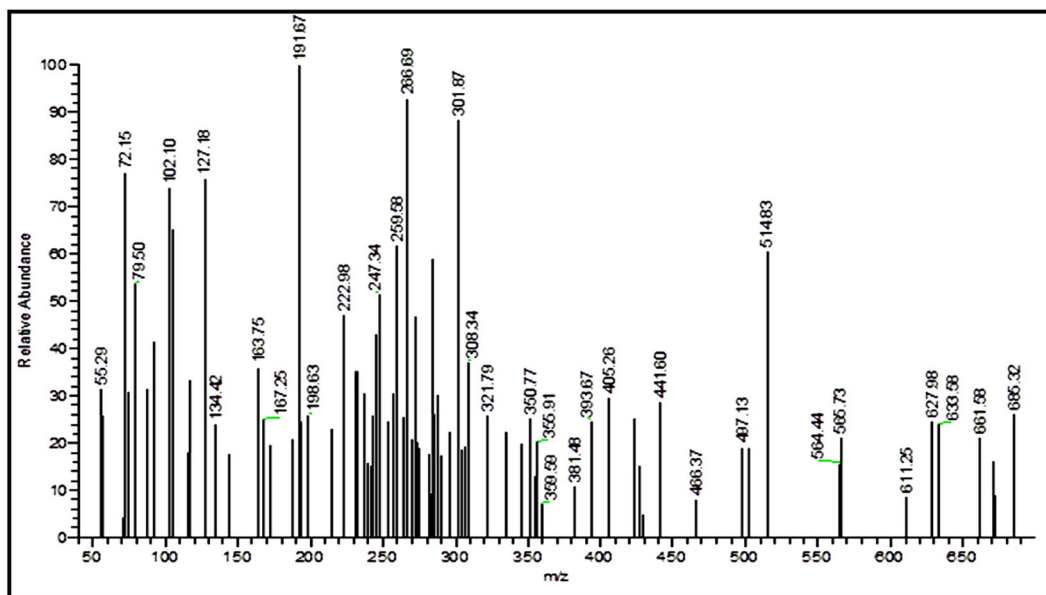


FIGURE 7 Mass spectrum of complex **2**; $[\text{Cu}_2(\text{L})(\text{OAc})_3(\text{H}_2\text{O})_5] \cdot \text{H}_2\text{O}$

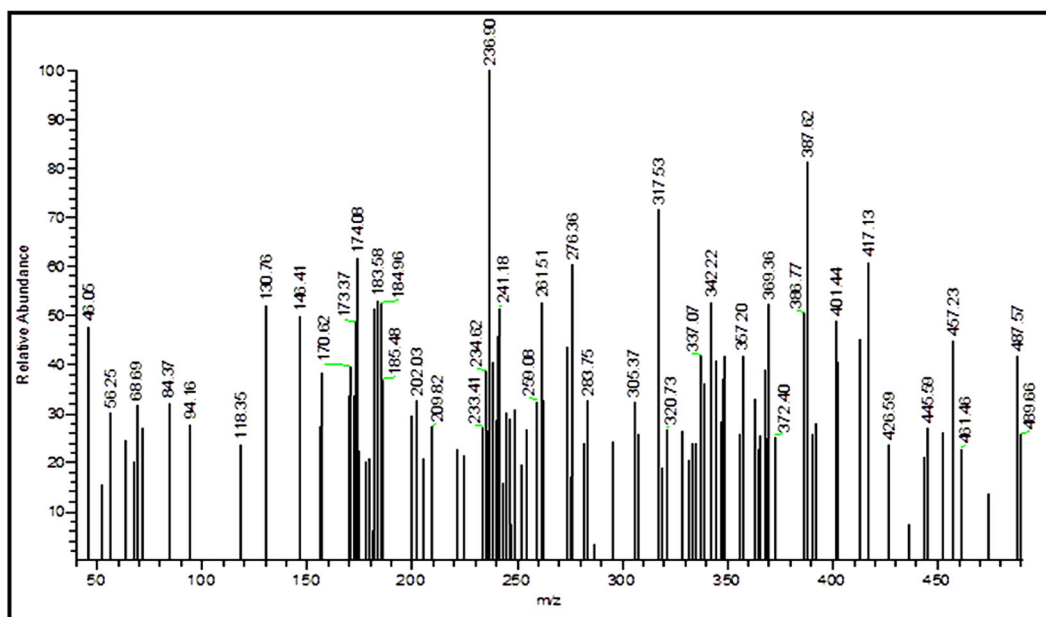


FIGURE 8 Mass spectrum of complex **4**; $[\text{Cu}(\text{HL})(\text{SO}_4)(\text{H}_2\text{O})_2] \cdot 2\text{H}_2\text{O}$

which is more reactive, and 3.620 eV for complex **4**, which is less reactive (more stable). This order agrees with the positive slope of E_{gap} versus $\Delta\nu_{\text{C}=\text{O}} \text{ cm}^{-1}$ mentioned in IR section that is well-matched with that obtained from E_{LUMO} versus $\Delta\nu_{\text{C}=\text{O}}/\text{cm}^{-1}$. Moreover, the relation of the dipole moment (μ) versus the shift of the stretching frequency of the C=O group (analogous of high stability of complex) is $\mu/D = -1.986 + 0.590 \Delta\nu_{\text{C}=\text{O}}/\text{cm}^{-1}$, $r = 0.95$, $n = 5$, except **3** and **4**, indicating an increase of complex polarity with the increasing of complex stability.

From Table 8 (Figure 14), the values of E_{gap} for the copper complexes were found to be 2.842, 0.436, 2.939, 3.620, 2.708, 3.374, and 1.956 eV. In all copper complexes, energy gap (E_{gap}) was small, which indicated the high reactivity of the prepared complexes. So the reactivity order of the compounds are **2** > **7** > **5** > **1** > **3** > **6** > **4** > **HL**, which agrees with anti-tumor results (*vide infra*), $E_{\text{gap}} = 2.410 + 0.0966 \text{ IC}_{50}$, $r = 0.86$, $n = 6$, except complex **1**. The positive slope indicates a decrease in the antitumor activity (IC_{50}) with the

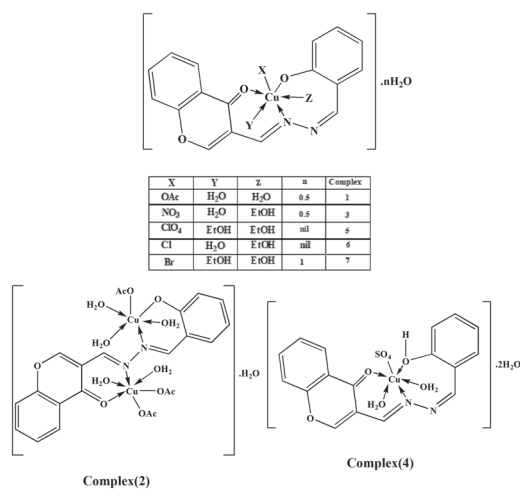


FIGURE 9 Representative structures of the prepared complexes

increase in stability of the complex (E_{gap}). Similar trend is obtained from E_{LUMO} versus IC_{50} , $E_{\text{LUMO}}/\text{eV} = -3.757 + 0.1345 \text{IC}_{50}$, $r = 0.97$, $n = 4$, except **HL** and complex **4**, whereas the high positive slope of E_{LUMO} with the IC_{50} indicates that the electron-donating groups are favorable for the activity.

3.3.1 | Structure–activity analysis

The inhibitory activity (IC_{50}) values of the current complexes, as usual, were changed to $\log 1/\text{IC}_{50}$ (pIC_{50}) to be in practical use in the analysis, which is modeled by using a linear regression technique. Linear regression analyses were carried out for gas phase by considering the experimental cytotoxic activity pIC_{50} as a dependent variable and the DFT-based global reactivity descriptors

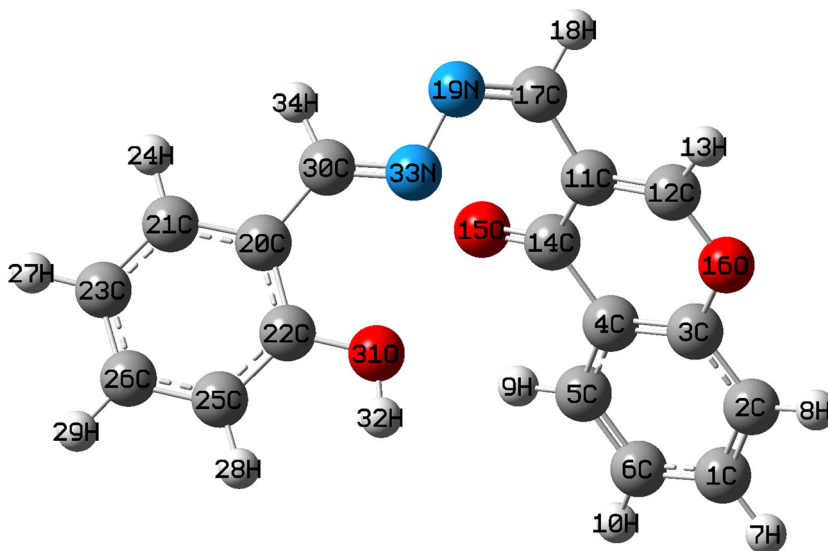


FIGURE 10 Molecular modeling of hydrazone ligand (HL)

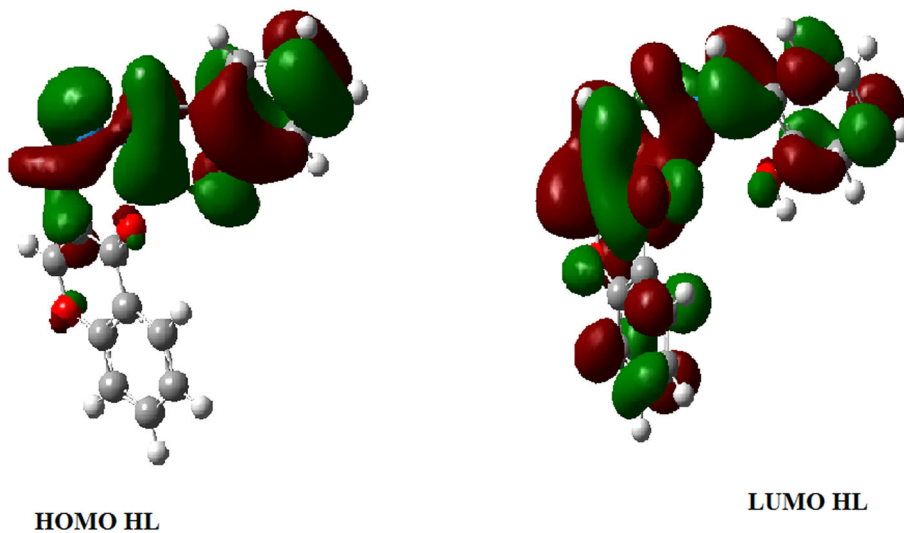


FIGURE 11 The electron density of highest occupied molecular orbital (HOMO) and lowest unoccupied molecular orbital (LUMO) of hydrazone ligand (HL)

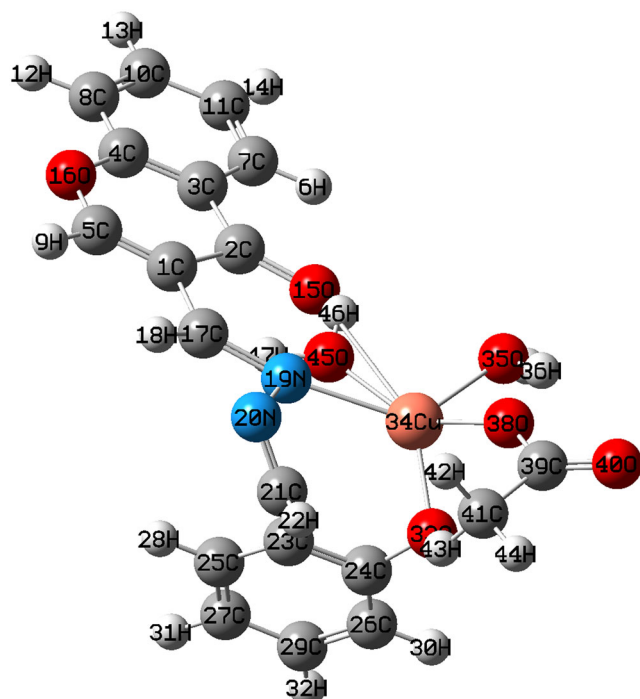


FIGURE 12 Molecular modeling of Cu(II) complex 1

obtained from BLYP/DNP method as an independent variable.

The positive value of absolute electronegativity (χ) and the negative value of chemical potential (μ) indicate that the complexes can accept electrons from the environment thereby decreasing its energy.^[61]

Furthermore, increasing the dipole moment (μ) values of the complexes improved the potent biological activities of the complexes. The dipole moment (μ) is found in the range 4.021–15.266 D; the less polar one is complex 5, but the highest polar is complex 1.

The global electrophilicity (ω /eV) values that were estimated by using the electronegativity and chemical hardness parameters (Table 8) are found in the range: 5.402–36.704 eV.^[59] Since the global electrophilicity (ω /eV) is a useful reactivity descriptor that can be used to compare the electron-donating abilities of molecules,^[62] that is, a high value of electrophilicity describes a good electrophile whereas a small value of electrophilicity describes a poor nucleophile,^[63] so the poor electrophile of the current complexes is the complex 6, while the good electrophile is complex 2. It is observed that reactivity descriptors calculated in the gas phase help to predict the cytotoxic activity of the complexes, indicating the importance of this model in the study of biomolecules. The modeled regression equation in the gas phase is given by a plot between the experimental pIC_{50} and calculated reactivity descriptors of the complexes—given in Table 8—shows that the electrophilicity indices (ω) are capable of predicting the cytotoxicity in a reasonable way; $\text{pIC}_{50} = -1.818 + 0.180 \omega/\text{eV}$, $r = 0.89$, $n = 5$, except complex 2.

The chelation of FCSH ligand can occur through the nitrogen atoms of hydrazono group N19, the oxygen atom of C=O group (chromone) O15, and O31 (OH group) as tridentate ligand except complex 2 “binuclear complex.” The net charge on coordinating centers in the chelating agent (HL) and its complexes are summarized in Table 9. The charges accumulated on O15 and O31 are -0.317 and -0.319 and on N19 and N33 are -0.136 and -0.287 , respectively. These values of charges suggest the chelation through the O15 and O31 of keto, N19, and N33 of the hydrazone. The quantity of charge migrated from the chelating agent to the metal ion (HL \rightarrow M) is shown in Table 9. The data indicated that the metal ion received apparent electronic charge from

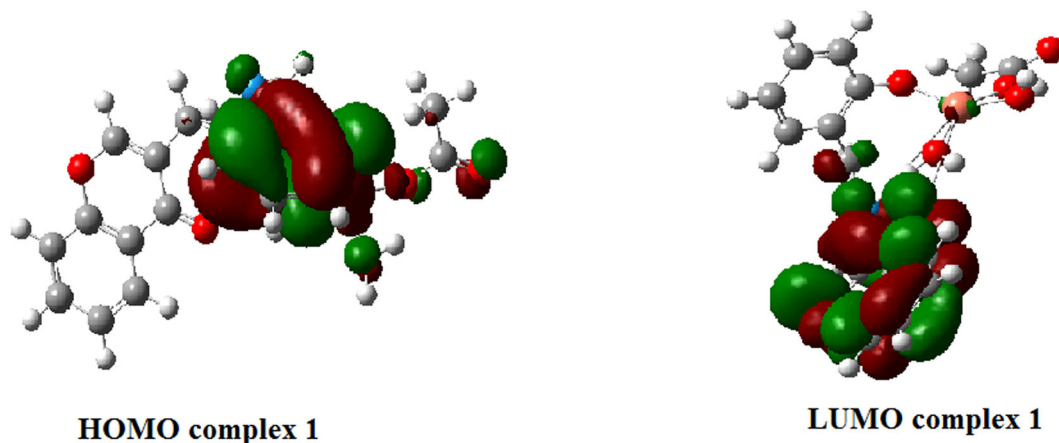


FIGURE 13 The electron density of highest occupied molecular orbital (HOMO) and lowest unoccupied molecular orbital (LUMO) of Cu(II) complex 1

TABLE 8 Total energy (au), energy of HOMO (eV), of LUMO (eV), energy gap (eV), electronegativity (eV), hardness (eV), electrophilicity (eV), softness (eV^{-1}) and dipole moment (Debye) for the HL ligand and its Cu(II) complexes using B3LYP/6-311G(d,p) level

Compounds	E_{Total} (au)	E_{HOMO} (eV)	E_{LUMO} (eV)	ΔE (eV)	χ (eV)	η (eV)	σ (eV^{-1})	π (eV)	S (eV^{-1})	ω (eV)	ΔN_{max}	Dipole (Debye)
HL	-990.38918	-5.959	-1.796	4.163	3.878	2.082	0.480	-3.878	0.240	3.609	1.863	4.0789
1	-3.010.8619	-5.492	-2.650	2.842	4.071	1.421	0.704	-4.071	0.352	5.834	2.865	15.2669
2	-5.337.2806	-4.218	-3.782	0.436	4.00	0.218	4.587	-4.00	2.294	36.704	18.349	11.2879
3	-3.065.4002	-6.014	-3.075	2.939	4.545	1.470	0.680	-4.545	0.340	7.023	3.092	8.4287
4	-3.482.4179	-6.423	-2.803	3.620	4.613	1.810	0.552	-4.613	0.276	5.873	2.549	15.6612
5	-3.548.4944	-6.311	-3.603	2.708	4.957	1.354	0.739	-4.957	0.370	9.092	3.661	4.0211
6	-3.229.6057	-5.959	-2.585	3.374	4.272	1.687	0.593	-4.272	0.296	5.402	2.532	11.4231
7	-5.359.5655	-5.628	-3.672	1.956	4.650	0.978	1.022	-4.650	0.511	11.050	4.755	14.1717

Abbreviations: HOMO, highest occupied molecular orbital; LUMO, lowest unoccupied molecular orbital; HL, hydrazone ligand.

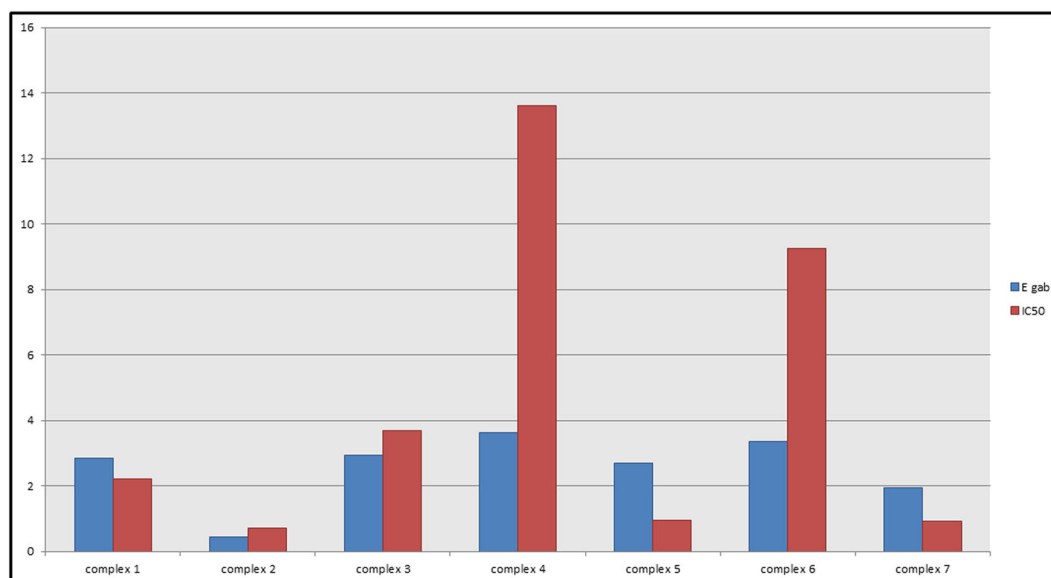


FIGURE 14 Relation between energy gap of the complexes and their antitumor activity

TABLE 9 The selected bond lengths and charge of Cu(II)complexes of HL ligand

Compounds	Charges					Bond length				
	O15 Chrom	O31 OH	N19 C=N chr	N33 C=N	Cu	C=O (15)	C-O (31) phenolic	C=N (19)	C=N (33)	N-N
HL	-0.317	-0.319	-0.136	-0.287	—	1.219	1.355	1.279	1.278	1.389
1	-0.457	-0.782	-0.349	-0.213	0.875	1.256	1.352	1.293	1.298	1.422
2	-0.547	-0.657	-0.368	-0.282	0.824	1.268	1.337	1.295	1.300	1.414
3	-0.450	-0.580	-0.293	-0.230	0.774	1.257	1.349	1.298	1.295	1.369
4	-0.467	-0.503	-0.189	-0.680	1.293	1.263	1.275	1.293	1.371	1.386
5	-0.442	-0.565	-0.218	-0.238	0.564	1.256	1.320	1.296	1.307	1.353
6	-0.561	-0.476	-0.296	-0.362	0.671	1.257	1.321	1.285	1.296	1.473
7	-0.482	-0.683	-0.184	-0.252	0.498	1.263	1.356	1.288	1.295	1.473

FCSH ligand (HL) proposing the great back donation from metal ion to the donation centers, revealing rises in the charge density on the donation site. The magnitude on the O15 and O31 donor atom of the HL (-0.317 and -0.319) increases in all complexes (natural charges range from -0.442 to -0.561 and from -0.476 to 0.782 for O15 and O31, respectively). This shows that HL-to-metal back donation of electrons happens through O15. However, N19 donor atom of ligand HL - 0.136 increases in all complexes to the range -0.189 to -0.368, showing that HL-to-metal back donation of electrons happens through N19.

The selected bond lengths extracted from the optimized structures are reported in Table 9. The bond lengths of the free ligand, HL, in the vicinity of coordinating centers are generally more or less elongated for most

complexes. The theoretical data in Table 9 showed that elongation of C=O15 (1.219 of HL) and C-O31 (1.355 of HL) to become in the range 1.256 to 1.268 Å and 1.275 to 1.356 Å, respectively, in all complexes. Also, elongation of C=N19 (1.279 of HL) to become in the range 1.285 to 1.298 Å in all complexes. While elongation of C=N33 (1.278 of HL) to become 1.300 Å for complex 2. This elongation observed at coordinating centers confirmed the coordination of HL with copper ion via C=O15, C-O31, and C=N19.^[64]

3.4 | Anticancer activity

The antitumor activity of FCSH and its complexes was examined in vitro against human hepatocellular

carcinoma (HepG-2) cell line. Doxorubicin (DOX), which is one of the most potent anticancer agents, was employed as reference drug. The activity results are expressed as IC_{50} , which is the compound concentration (in $\mu\text{g/ml}$) that inhibits a proliferation rate of the tumor cells by 50% as compared with control untreated cells (Table 10).

The obtained results illustrated that FCSH and all the synthesized complexes exhibited a growth inhibition activity on the tested cell line. FCSH exhibited weak activity ($IC_{50} = 123 \mu\text{g/ml}$), but all complexes are more active with strong activity. Complexes **2**, **5**, and **7** exhibited the strongest activity ($IC_{50} = 0.7\text{--}0.92 \mu\text{g/ml}$), which is close to that of the reference anticancer; doxorubicin ($IC_{50} = 0.36 \mu\text{g/ml}$). Also, complexes **1**, **3**, **4**, and **6** exhibited moderate activity ($IC_{50} = 2.21\text{--}13.6 \mu\text{g/ml}$). The potent activity of the complexes than FCSH ligand may have arisen from the increased conjugation occurring in FCSH skeleton owing to complexation process.^[65] The order of activity is: acetate (binuclear) > bromide > perchlorate > acetate (mononuclear) > nitrate > chloride > sulfate. This order reflects that the reactive complex (lower E_{gap}) is highly reactive antitumor (lower IC_{50}). Since the stability of complex also depends upon the Lewis basicity of anion (DN_x), the type of anion affects the antitumor activity of the present complexes.

However, the mechanism of action is complicated as the current system consists of a heterocyclic ligand (FCSH) with various coordinating sites giving an opportunity of interaction either with nucleoside bases or with biologically important metal ions that exist in the biosystem.^[66] Apart from this mechanism of action, the investigated compounds may form H bonds via the coordinated anions in addition to the azomethine group, with the active centers of the cell constituents leading to an interference with the normal cell process.^[67] Thus, we can conclude that anion coordination affects the antitumor activity of the synthesized complexes.

TABLE 10 Antitumor activity of the ligand and its Cu(II) complexes

Compound	IC_{50} ($\mu\text{g/ml}$)	
HL	123 ± 6.2	
1	$[Cu(L)(OAc)(H_2O)_2] \cdot 0.5H_2O$	2.21 ± 0.29
2	$[Cu_2(L)(OAc)_3(H_2O)_5] \cdot H_2O$	0.70 ± 0.02
3	$[Cu(L)(NO_3)(EtOH)(H_2O)] \cdot 0.5H_2O$	3.68 ± 0.18
4	$[Cu(HL)(SO_4)(H_2O)_2] \cdot 2H_2O$	13.6 ± 1.4
5	$[Cu(L)(ClO_4)(EtOH)_2]$	0.96 ± 0.03
6	$[Cu(L)Cl(EtOH)(H_2O)]$	9.25 ± 0.64
7	$[Cu(L)Br(EtOH)_2] \cdot H_2O$	0.92 ± 0.02
Doxorubicin	0.36 ± 0.04	

The correlations containing the descriptors derived from this model show that there are no collinearity problems between descriptors (Table 8). The equation describing the IC_{50} for this model contains the E_{HOMO} , E_{LUMO} , and electronic descriptors. The obtained statistical model has a correlation coefficients r in the range 0.82–0.99, which supports the reliability and goodness of the model.

The main points of interest from the linear regression of pIC_{50} versus the structural parameters and reactivity descriptors are as follows:

- E_{HOMO} indicates the importance of electrostatic interactions of the ligand with an enzyme when a molecule acts as electron pair donor in bond formation; the electrons are supplied from the HOMO of the molecule. HOMO descriptor denotes the nucleophilicity of the molecules, $pIC_{50} = -4.407 + 5.827$ nucleophilicity/eV, $r = 0.98$, $n = 5$, except complexes **2** and **7**. The highest positive coefficient in the equation indicates that the increase in the electron energy of the molecules increases the activity.
- Energy of low molecular orbital measures the electrophilicity of the molecule. The high positive correlation of LUMO with the IC_{50} indicates that the electron-donating groups are favorable for the activity.
- Dipole moment is negatively correlated with the inhibition activity with a small coefficient.
- The hardness (η/eV) measures the stability of complexes, $pIC_{50} = 1.7524 - 1.5446 \eta/\text{eV}$, $r = 0.91$, $n = 6$, except complex **2**. The negative slope indicates that a less reactive complex has high antitumor activity. This is emphasized by the positive slope of softness that measures the reactivity of complex; $pIC_{50} = -4.387 + 11.595 S/\text{eV}$, $r = 0.98$, $n = 5$, except complexes **2** and **7**.
- The electronegativity (χ/eV) of complex enhanced its antitumor activity as indicated from the positive slope of pIC_{50} versus χ , $pIC_{50} = -7.361 + 1.518 \chi/\text{eV}$, $r = 0.88$, $n = 4$, except complexes **1**, **2**, and **4**. The increasing of χ and ω might be attributed to the enhancement of conjugation in the ligand skeleton upon complexation and may be the reason for improved antitumor activity.

It is concluded from the DFT calculations that the calculated quantum chemical parameters could explain the factors affecting on the IC_{50} of the investigated compounds, which is in a good agreement with the experimental observations. Structure–activity relationship study shows that E_{HOMO} , E_{gap} , hardness, and ionization potential are the most significant descriptors for the correlation with the IC_{50} .

Finally, the present study shows that the quantum chemical parameters and molecular docking analysis are successful tools for better description of IC_{50} .

3.5 | Molecular docking study

Molecular docking simulation is one of the most important methods to expect the inhibitory potential

and the binding mode as well as mechanistic information of chemical moieties in the pocket of the enzyme. It is a reliable computational protocol that can be employed to suppose the interactions between synthesized compounds and enzyme receptors. Furthermore, it is used to investigate the optimized orientations and binding features of any molecule that results in a new complex with total minimum energy.^[68,69]

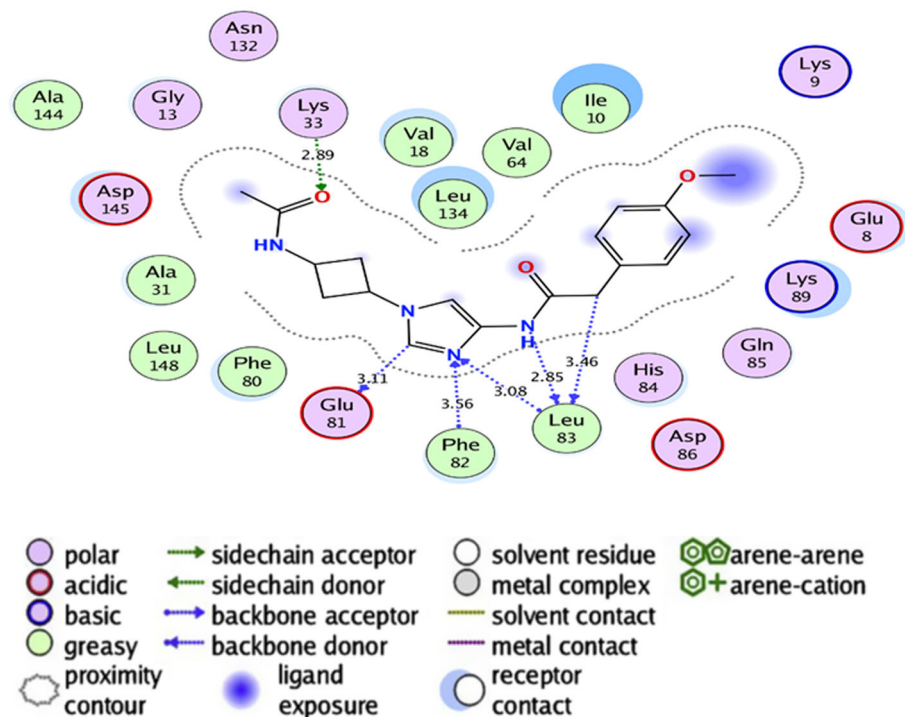


FIGURE 15 2D interaction diagram showing the co-crystallized ligand docking pose interactions with the key amino acids in CDK-2 binding site (PDB: 3IG7)

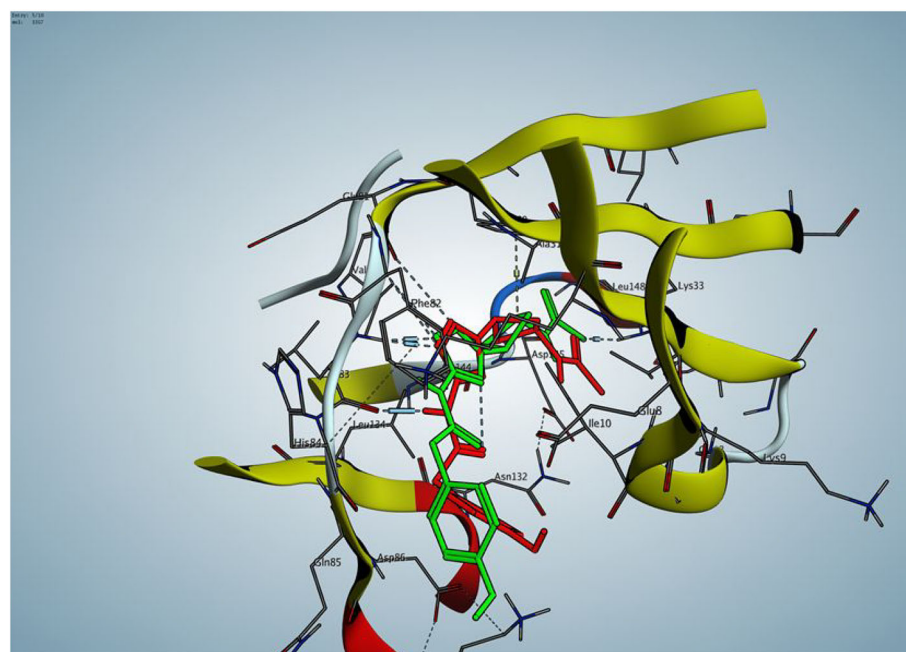


FIGURE 16 3D representation of the superimposition of the co-crystallized (red) and the docking pose (green) of the ligand in CDK-2 binding site with RMSD of 1.7453 Å

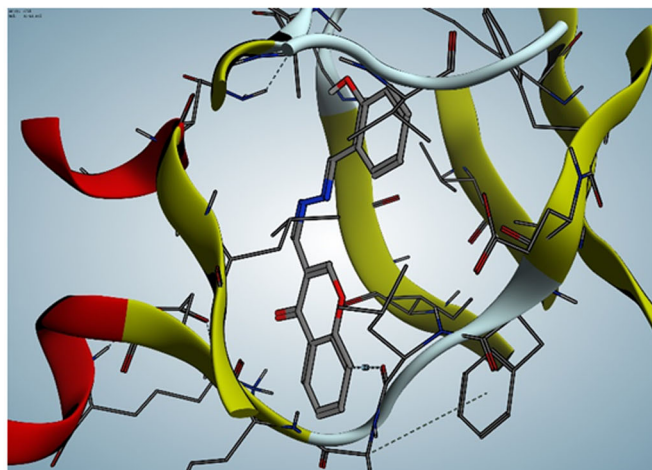
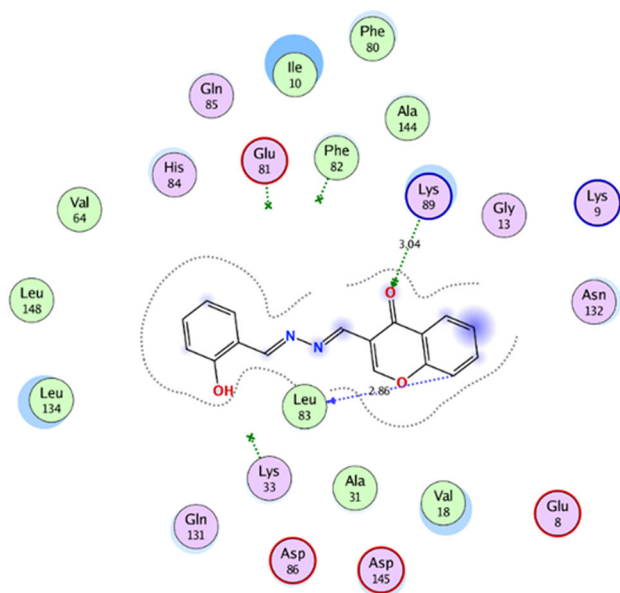


FIGURE 17 2D and 3D diagrams of hydrazone ligand (HL) showing its interaction with the tyrosine CDK-2 binding site

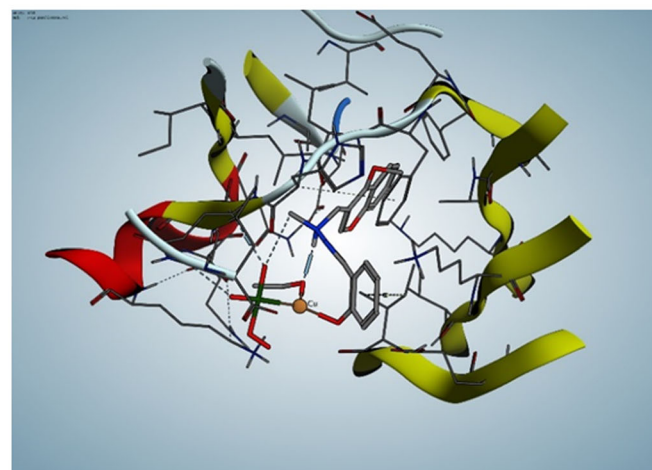
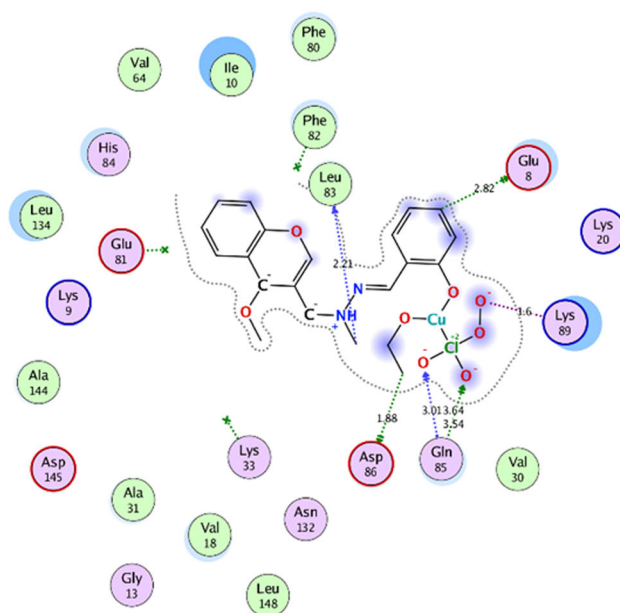


FIGURE 18 2D and 3D diagrams of complex 5 showing its interaction with the tyrosine CDK-2 binding site

In the present work, PDB ID: 31G7 was used, which has CDK-2 co-crystallized with the *N*-{1-[*cis*-3-(acetyl-amino)cyclobutyl]-1*H*-imidazol-4-yl]-2-(4-methoxyphenyl)acetamide as inhibitor.

Validation of the molecular docking protocol was first achieved by self-docking of the co-crystallized ligand, *N*-{1-[*cis*-3-(acetyl-amino)cyclobutyl]-1*H*-imidazol-4-yl]-2-(4-methoxyphenyl)acetamide, in the CDK-2 active site. The self-docking validation step reproduced the experimental binding pattern of the co-crystallized ligand efficiently

demonstrating the suitability of the used docking setup for the planned docking study as evidenced by a binding score of -11.2371 kcal/mol and the small RMSD of 1.7453 Å between the docking pose and the co-crystallized ligand (according to the literature,^[70] if the RMSD of the best docked conformation of the native ligand is ≤ 2.0 Å from the experimental one, the used scoring function is successful) and by its ability to reproduce all the key interactions accomplished by the co-crystallized ligand with the key amino acids (hot spots) in the active

TABLE 11 Docking results of the hydrazone ligand and its Cu(II) complexes

Compound	S (kcal/mol)	Amino acids	Interacting groups	Type of interaction	Length
HL	−11.0562	Leu83	CH (Arom.)	Side chain donor	2.86
		Lys89	O (C=O)	Backbone acceptor	3.04
1 [Cu(L)(OAc)(H ₂ O) ₂].0.5H ₂ O	−10.8693	Lys33	=N	Backbone acceptor	2.21
		Asp145	=CH	Backbone donor	2.00
		Asp145	CH ₃	Backbone donor	2.67
2 [Cu ₂ (L)(OAc) ₃ (H ₂ O) ₅].H ₂ O	−10.1109	Asp86	NH	Backbone donor	2.85
		Lys89	O (C=O)	Backbone acceptor	2.08
		Gln131	CH ₃	Side chain donor	3.19
3 [Cu(L)(NO ₃)(EtOH)(H ₂ O)].0.5H ₂ O	−11.1534	Lys33	O (O=N)	Backbone acceptor	3.14
		Asp86	CH ₃ (O)	Backbone donor	2.53
		Asp86	CH ₃ (N)	Backbone donor	2.98
		Lys89	C [−] (Pyran)	Ionic	3.23
		Gln131	CH ₃ (N)	Side chain donor	3.42
4 [Cu (HL)(SO ₄)(H ₂ O) ₂].2H ₂ O	−11.1212	Leu83	CH ₃ (N)	Side chain donor	3.43
		Asp86	CH (Arom.)	Backbone donor	3.56
		Lys89	C [−] (Pyran)	Ionic	3.92
5 [Cu(L)(ClO ₄)(EtOH) ₂]	−12.4192	Glu8	CH (Arom.)	Backbone donor	2.82
		Leu83	CH ₃ (N)	Side chain donor	2.21
		Gln85	O (Cl)	Backbone acceptor	3.54
		Gln85	O (Cl)	Side chain acceptor	3.01
		Asp86	CH ₃ (Et)	Backbone donor	1.88
		Lys89	O [−] (O-O)	Ionic	1.60
6 [Cu(L)Cl (EtOH)(H ₂ O)]	−10.6345	Leu83	OH	Side chain acceptor	2.45
		Leu83	CH ₃ (N)	Side chain donor	3.07
		Asp86	CH ₃ (O)	Backbone donor	3.00
		Lys89	C [−] (Pyran)	Ionic	3.25
7 [Cu(L)Br (EtOH) ₂].H ₂ O	−9.3017	Ile10	=CH	Side chain donor	3.30
		Lys89	C [−] (Pyran)	Ionic	2.83
		Gln131	Cu	Ionic	2.80
		Asn132	Br	Side chain donor	2.70
		Asn132	O	Backbone acceptor	2.59

site (Lys33, Glu81, Phen82, and Leu83). The results are represented in Figures 15 and 16. The function of molecular docking study is to expect the possible binding mode of FCSH ligand and its Cu(II) complexes and to investigate their interactions with the key amino acids (hot spots) in the active site of the CDK-2 enzyme with the aim of elucidation of their promising inhibitory activity.

Two- and three-dimensional structures of docking of the FCSH and complex **5**—as representative example—are shown in Figures 17 and 18. As observed from Figures 17 and 18, the synthesized compounds revealed that they docked well into the binding site and displayed

favorable interactions with the crucial amino acid residues.

Also, the binding energies of FCSH and its Cu(II) complexes were calculated using computational docking studies. These energy values were listed in Table 11. As indicated in Table 11, the current compounds have negative binding free energy, suggesting effective binding with protein. In addition, the molecular docking data revealed that FCSH and its complexes showed good binding interactions with the binding sites with a good binding score ranging from −9.3017 to −12.4192 kcal/mol (Table 11). The more negative relative binding energy of complex **7** suggests more ability to bind

to protein compared with the free ligand and other Cu(II) complexes.

4 | CONCLUSION

A new tridentate HL (FCSH) was synthesized by reaction of salicylaldehyde hydrazone with 3-formylchromone. Reactions of the ligand with different copper(II) salts yielded seven complexes, which were characterized by several analytical and spectroscopic methods. The ligand behaves as monobasic tridentate for all complexes except complex **2** (monobasic tetradentate) and complex **4** (neutral tridentate). The coordinating sites are phenolic oxygen, azomethine nitrogen, and γ -pyrone oxygen atoms. By using of Coats–Redfern equations, the kinetic parameters of the thermal decomposition stages were calculated and discussed. At the B3LYP/6-311G(d,p) level engaged in the *Gaussian 09* program, DFT calculations were carried out to inspect the optimized structures of the chelating agent and its complexes. The ligand and its copper(II) complexes showed antitumor activity towards HepG2 cell line. The docking study of FCSH and its Cu(II) complexes was reported. Docking results showed that FCSH and its complexes showed good binding interactions with the binding sites with a good binding score.

AUTHOR CONTRIBUTIONS

Ebtesam M. Abdelrhman: Data curation; investigation. **B.A. El-Shetary:** Conceptualization; supervision; validation; visualization. **Magdy Shebl:** Conceptualization; supervision; validation; visualization. **Omima M.I. Adly:** Conceptualization; methodology; supervision; validation; visualization.

ORCID

Ebtesam M. Abdelrhman  <https://orcid.org/0000-0002-3712-6948>

B.A. El-Shetary  <https://orcid.org/0000-0002-9359-296X>

Magdy Shebl  <https://orcid.org/0000-0003-4377-2273>

Omima M.I. Adly  <https://orcid.org/0000-0003-0197-8118>

REFERENCES

- [1] a) A. Ray, S. Banerjee, S. Sen, R. J. Butcher, G. M. Rosair, M. T. Garland, S. Mitra, *Struct. Chem.* **2008**, *19*, 209; b) S. A. Aboafia, S. A. Elsayed, A. K. A. El-Sayed, A. M. El-Hendawy, *J. Mol. Struct.* **2018**, *1158*, 39.
- [2] a) G. A. A. Al-Hazmi, K. S. Abou-Melha, N. M. El-Metwaly, I. Althagafi, F. Shaaban, M. G. Elghalban, M. M. El-Gamil, *Appl. Organometal. Chem.* **2020**, *34*, e5408; b) A. Zülfikaroğlu, Ç. Y. Ataol, E. Çelikoğlu, U. Çelikoğlu, Ö. İdil, *J. Mol. Struct.* **2020**, *1199*, 127012.
- [3] a) M. S. S. Adam, M. S. M. Ahmed, O. M. El-Hady, S. Shaaban, *Appl. Organometal. Chem.* **2020**, *34*, e5573; b) O. A. El-Gammal, G. M. Abu El-Reash, R. A. Bedier, *Appl. Organometal. Chem.* **2019**, *33*, e5141.
- [4] a) Y. Burgos-Lopez, J. Del Pla, L. M. Balsaa, I. E. Leon, G. A. Echeverri, O. E. Piro, J. Garcia-Tojal, R. Pis-Diez, A. C. Gonzalez-Baro, B. S. Parajon-Costa, *Inorg. Chim. Acta* **2019**, *487*, 31; b) I. Babahan, A. Özmen, M. Aksel, M. D. Bilgin, R. Gumusada, M. E. Gunay, F. Eyduvan, *Appl. Organometal. Chem.* **2020**, *34*, e5632.
- [5] O. I. El-Sabbagh, H. M. Rady, *Eur. J. Med. Chem.* **2009**, *44*, 3680.
- [6] G. S. Hegde, S. P. Netalkar, V. K. Revankar, *Appl. Organometal. Chem.* **2019**, *33*, e4840.
- [7] R. P. Bakale, G. N. Naik, C. V. Mangannavar, I. S. Muchchandi, I. N. Shcherbakov, C. Frampton, K. B. Gudasi, *Eur. J. Med. Chem.* **2014**, *73*, 38.
- [8] a) P. Sathyadevi, P. Krishnamoorthy, M. Alagesan, K. Thanigaimani, P. T. Muthiah, N. Dharmaraj, *Polyhedron* **2012**, *31*, 294; b) M. Shebl, S. M. E. Khalil, M. A. A. Kishk, D. M. El-Mekki, M. Saif, *Appl. Organometal. Chem.* **2019**, *33*, e5147; c) R. Gup, C. Gökce, N. Dilek, *J. Photochem. Photobiol., B* **2015**, *144*, 42.
- [9] J. E. Philip, S. A. Antony, S. J. Eeetinilkunnathil, M. R. P. Kurup, M. P. Velayudhan, *Inorg. Chim. Acta* **2018**, *469*, 87.
- [10] a) A. A. Alothman, M. D. Albaqami, *Appl. Organometal. Chem.* **2020**, *34*, e5827; b) M. Shebl, M. Saif, A. I. Nabeel, R. Shokry, *J. Mol. Struct.* **2016**, *1118*, 335.
- [11] D. P. Ilboudo, N. Basilico, S. Parapini, Y. Corbett, S. D'Alessandro, M. Dell'Agli, P. Coghi, S. D. Karou, R. Sawadogo, C. Gnoula, J. Simpoire, J.-B. Nikiema, D. Monti, E. Bosisio, D. Taramelli, *J. Ethnopharmacol.* **2013**, *148*, 763.
- [12] M. Gaber, K. El-Baradie, N. El-Wakiel, S. Hafez, *Appl. Organometal. Chem.* **2020**, *34*, e5348.
- [13] Q. Liu, X. Qiang, Y. Li, Z. Sang, Y. Li, Z. Tan, Y. Deng, *Bioorg. Med. Chem.* **2015**, *23*, 911.
- [14] a) Y. S. Shim, K. C. Kim, D. Y. Chi, K. Lee, H. Cho, *Bioorg. Med. Chem. Lett.* **2003**, *13*, 2561; b) J. E. Philip, M. Shahid, M. R. P. Kurup, M. P. Velayudhan, *J. Photochem. Photobiol., B* **2017**, *175*, 178.
- [15] a) E. Salvadeo, L. Dubois, J.-M. Latour, *Coord. Chem. Rev.* **2018**, *374*, 345; b) K. M. Takroni, T. A. Farghaly, M. F. Harras, H. A. El-Ghamry, *Appl. Organometal. Chem.* **2020**, *34*, e5860; c) M. Shebl, *Spectrochim. Acta a* **2014**, *117*, 127; d) C. Elamathi, R. Butcher, R. Prabhakaran, *Appl. Organometal. Chem.* **2019**, *33*, e4659; e) N. Zare, A. Zabardasti, *Appl. Organometal. Chem.* **2019**, *33*, e4687.
- [16] S. M. El-Medani, M. M. Aboaly, H. H. Abdalla, R. M. Ramadan, *Spectroscopy Lett.* **2004**, *37*, 619.
- [17] A. Nohara, T. Umetani, Y. Sanno, *Tetrahedron* **1974**, *30*, 3553.
- [18] F. E. Mabbs, D. I. Machin, *Magnetism and Transition Metal Complexes*, Chapman and Hall, London **1973**.
- [19] M. J. Frisch, G. W. Trucks, H. B. Schlegel, G. E. Scuseria, M. A. Robb, J. R. Cheeseman, G. Scalmani, V. Barone, B. Mennucci, G. A. Petersson, H. Nakatsuji, M. Caricato, X. Li, H. P. Hratchian, A. F. Izmaylov, J. Bloino, G. Zheng, J. L. Sonnenberg, M. Hada, M. Ehara, K. Toyota, R. Fukuda, J. Hasegawa, M. Ishida, T. Nakajima, Y. Honda, O. Kitao, H. Nakai, T. Vreven, J. A. Montgomery Jr., J. E. Peralta, F. Ogliaro, M. Bearpark, J. J.

- Heyd, E. Brothers, K. N. Kudin, V. N. Staroverov, R. Kobayashi, J. Normand, K. Raghavachari, A. Rendell, J. C. Burant, S. S. Iyengar, J. Tomasi, M. Cossi, N. Rega, J. M. Millam, M. Klene, J. E. Knox, J. B. Cross, V. Bakken, C. Adamo, J. Jaramillo, R. Gomperts, R. E. Stratmann, O. Yazyev, A. J. Austin, R. Cammi, C. Pomelli, J. W. Ochterski, R. L. Martin, K. Morokuma, V. G. Zakrzewski, G. A. Voth, P. Salvador, J. J. Dannenberg, S. Dapprich, A. D. Daniels, O. Farkas, J. B. Foresman, J. V. Ortiz, J. Cioslowski, D. J. Fox, Gaussian Inc., Wallingford, CT. **2009**.
- [20] T. Mosmann, *J. Immunol. Methods* **1983**, 65, 55.
- [21] S. M. Gomha, S. M. Riyadh, E. A. Mahmmoud, M. M. Elaasser, *Heterocycles* **2015**, 91, 1227.
- [22] rcsb PDB Homepage <https://www.rcsb.org/>
- [23] a) B.-d. Wang, Z.-Y. Yang, M.-h. Lü, J. Hai, Q. Wang, Z.-N. Chen, *J. Organomet. Chem.* **2009**, 694, 4069; b) B.-d. Wang, Z.-Y. Yang, T.-r. Li, *Bioorg. & Med. Chem.* **2006**, 14, 6012.
- [24] M. Shebl, *Spectrochim. Acta a* **2008**, 70, 850.
- [25] D.-C. Ilies, E. Pahontu, S. Shova, R. Georgescu, N. Stanica, R. Olar, A. Gulea, T. Rosu, *Polyhedron* **2014**, 81, 123.
- [26] M. Shebl, *J. Coord. Chem.* **2009**, 62, 3217.
- [27] H. F. Abd El-Halim, G. G. Mohamed, M. N. Anwar, *Appl. Organometal. Chem.* **2018**, 32, e3899.
- [28] K. Nakamoto, *Infrared and Raman Spectra of Inorganic and Coordination Compounds*, 5th ed., John Wiley and Sons, New York **1997**.
- [29] a) H. El-Ghamry, N. El-Wakiel, A. Khamis, *Appl. Organometal. Chem.* **2018**, 32, 4583; b) H. S. Seleem, B. A. El-Shetary, M. Shebl, *Heteroatom. Chem.* **2007**, 18, 100; c) M. Shebl, *J. Coord. Chem.* **2016**, 69, 199.
- [30] F. Samy, M. Shebl, *Appl. Organometal. Chem.* **2020**, 34, e5502.
- [31] H. F. El-Shafiy, M. Shebl, *J. Mol. Struct.* **2019**, 1194, 187.
- [32] F. Hueso-Ureña, M. N. Moreno-Carretero, A. L. Peñas-Chamorro, J. M. Amigó, V. Esteve, T. Debaerdemaeker, *Polyhedron* **1999**, 18, 3629.
- [33] M. M. Hassanien, I. M. Gabr, M. H. Abdel-Rhman, A. A. El-Asmy, *Spectrochim. Acta a* **2008**, 71, 73.
- [34] a) M. Shebl, *Spectrochim. Acta a* **2009**, 73, 313; b) E. M. Saad, M. S. El-Shahwai, H. Saleh, A. A. El-Asmy, *Trans. Met. Chem* **2007**, 32, 155; c) M. Shebl, H. S. Seleem, B. A. El-Shetary, *Spectrochim. Acta a* **2010**, 75, 428.
- [35] a) M. Gaber, N. El-Wakiel, K. El-Baradie, S. Hafez, *J. Iran. Chem. Soc.* **2019**, 16, 169; b) M. Shebl, S. M. E. Khalil, *Monatsh. Chem.* **2015**, 146, 15.
- [36] W. J. Geary, *Coord. Chem. Rev.* **1971**, 7, 81.
- [37] S. M. E. Khalil, M. Shebl, F. S. Al-Gohani, *Acta Chim. Slov.* **2010**, 57, 716.
- [38] M. Shebl, S. M. E. Khalil, F. S. Al-Gohani, *J. Mol. Struct.* **2010**, 980, 78.
- [39] G. A. A. Al-Hazmi, M. S. El-Shahawi, I. M. Gabr, A. A. El-Asmy, *J. Coord. Chem.* **2005**, 58, 713.
- [40] N. M. El-Metwally, I. M. Gabr, A. M. Shallaby, A. A. El-Asmy, *J. Coord. Chem.* **2005**, 58, 1145.
- [41] K. S. Abu-Melha, N. M. El-Metwally, *Spectrochim. Acta a* **2008**, 70, 277.
- [42] W. H. Mahmoud, R. G. Deghadi, G. G. Mohamed, *J. Therm. Anal. Calorim.* **2017**, 127, 2149.
- [43] M. Shebl, *J. Mol. Struct.* **2017**, 1128, 79.
- [44] J. P. Jasinski, J. R. Bianchani, J. Cuva, F. A. El-Said, A. A. El-Asmy, D. X. West, *Z. Anorg. Allg. Chem.* **2003**, 629, 202.
- [45] B. J. Hathaway, D. E. Billing, *Coord. Chem. Rev.* **1970**, 5, 143.
- [46] B. J. Hathaway, *Struct. Bonding* **1984**, 57, 55.
- [47] E. Garribba, G. Micera, *J. Chem. Ed.* **2006**, 83, 1229.
- [48] C. J. Carrano, C. M. Nunn, R. Quan, J. A. Bonadies, V. L. Pecoraro, *Inorg. Chem.* **1990**, 29, 944.
- [49] B. Jeragh, A. A. El-Asmy, *Spectrochim. Acta a* **2014**, 129, 307.
- [50] a) H. F. El-Shafiy, *J. Mol. Struct.* **2018**, 1166, 348; b) S. A. Sadeek, S. M. Abd El-Hamid, W. A. Zordok, *Appl. Organometal. Chem.* **2018**, 32, e4457; c) H. F. El-Shafiy, M. Shebl, *J. Mol. Struct.* **2018**, 1156, 403.
- [51] A. W. Coats, J. P. Redfern, *Nature* **1964**, 201, 68.
- [52] A. H. M. Siddaligaiah, S. G. Naik, *J. Mol. Struct.* **2002**, 582, 129.
- [53] C. R. Vinodkumar, M. K. Muraleedharan Nair, P. K. Radhakrishnan, *J. Therm. Anal. Cal.* **2000**, 61, 143.
- [54] U. El-Ayaan, I. M. Gabr, *Spectrochim. Acta a* **2007**, 67, 263.
- [55] W.-Y. Wang, X.-F. Du, N.-N. Ma, S.-L. Sun, Y.-Q. Qiu, *J. Mol. Model.* **2013**, 19, 1779.
- [56] R. C. Maurya, B. A. Malik, J. M. Mir, P. K. Vishwakarma, D. K. Rajak, N. Jain, *J. Mol. Str.* **2015**, 1099, 266.
- [57] A. K. Chandra, T. Uchimara, *J. Phys. Chem. A* **2001**, 105, 3578.
- [58] A. A. H. Kadhum, A. A. Al-Amiery, M. Shikara, A. Mohamad, *Int. J. Phys. Sci.* **2011**, 6, 6692.
- [59] A. Z. El-Sonbati, M. A. Diab, A. A. El-Bindary, S. M. Morgan, *Spectrochim. Acta* **2014**, 127, 310.
- [60] T. A. Yousef, G. M. Abu El-Reash, O. A. El-Gammal, S. F. Ahmed, *Polyhedron* **2014**, 81, 749.
- [61] A. Y. Al Dawood, N. M. El Metwaly, H. A. El Ghamry, *J. Mol. Liq.* **2016**, 220, 311.
- [62] P. K. Chattaraj, U. Sarkar, D. R. Roy, *Chem. Rev.* **2006**, 106, 2065.
- [63] E. E. Ebenso, M. M. Kabanda, T. Arslan, M. Saracoglu, F. Kandemirli, L. C. Murulana, A. K. Singh, S. K. Shukla, B. Hammouti, K. F. Khaled, M. A. Quraishi, I. B. Obot, N. O. Edd, *Int. J. Electrochem. Sci.* **2012**, 7, 5643.
- [64] T. A. Yousef, *J. Mol. Struct.* **2020**, 1215, 128180.
- [65] K. Dhahagani, S. M. Kumar, G. Chakkaravarthi, K. Anitha, J. Rajesh, A. Ramu, G. Rajagopal, *Spectrochim. Acta a* **2014**, 117, 87.
- [66] Z. H. Chohan, H. Pervez, A. Rauf, K. M. Khan, C. T. Supuran, *J. Enz. Inhib. Med. Chem.* **2004**, 19, 417.
- [67] B. Murukan, B. S. Kumari, K. Mohanan, *J. Coord. Chem.* **2007**, 60, 1607.
- [68] P. Roobahani, M. Salehi, R. E. Malekshah, M. Kubicki, *Inorg. Chim. Acta* **2019**, 496, 119022.
- [69] S. W. Kattan, M. S. Nafie, G. A. Elmgeed, W. Alelwani, M. Badar, M. A. Tantawy, J. Steroid, *Biochem. Molec. Bio.* **2020**, 198, 105604.
- [70] P. Mahajan, G. Chashoo, M. Gupta, A. Kumar, P. P. Singh, A. Nargotra, *J. Chem. Inf. Model.* **2017**, 57, 195.

How to cite this article: Abdelrhman EM, El-Shetary BA, Shebl M, Adly OMI. Coordinating behavior of hydrazone ligand bearing chromone moiety towards Cu(II) ions: Synthesis, spectral, density functional theory (DFT) calculations, antitumor, and docking studies. *Appl Organomet Chem.* 2021;e6183. <https://doi.org/10.1002/aoc.6183>